JACS
JOURNAL OF THE AMERICAN CHEMICAL SOCIETY
Article
pubs.acs.org/JACS

Solid-State Synthesis and Characterization of σ-Alkane Complexes, $[Rh(L_2)(\eta^2,\eta^2\text{-}C_7H_{12})][BAr^F{}_4]$ (L_2 = Bidentate Chelating Phosphine)

Sebastian D. Pike,[†] F. Mark Chadwick,[†] Nicholas H. Rees,[†] Mark P. Scott,[†] Andrew S. Weller,*[,†] Tobias Krämer,[‡] and Stuart A. Macgregor*[,‡]

[†]Department of Chemistry, Chemistry Research Laboratories, University of Oxford, Mansfield Road, Oxford OX1 3TA, U.K.
[‡]Institute of Chemical Sciences, Heriot-Watt University, Edinburgh EH14 4AS, U.K.

Supporting Information

ABSTRACT: The use of solid/gas and single-crystal to single-crystal synthetic routes is reported for the synthesis and characterization of a number of σ-alkane complexes: $[Rh(R_2P(CH_2)_nPR_2)(\eta^2,\eta^2\text{-}C_7H_{12})][BAr^F{}_4]$; R = Cy, n = 2; R = ^{i}Pr, n = 2,3; Ar = 3,5-$C_6H_3(CF_3)_2$. These norbornane adducts are formed by simple hydrogenation of the corresponding norbornadiene precursor in the solid state. For R = Cy (n = 2), the resulting complex is remarkably stable (months at 298 K), allowing for full characterization using single-crystal X-ray diffraction. The solid-state structure shows no disorder, and the structural metrics can be accurately determined, while the ^{1}H chemical shifts of the Rh···H−C motif can be determined using solid-state NMR spectroscopy. DFT calculations show that the bonding between the metal fragment and the alkane can be best characterized as a three-center, two-electron interaction, of which $\sigma_{CH} \rightarrow$ Rh donation is the major component. The other alkane complexes exhibit solid-state ^{31}P NMR data consistent with their formation, but they are now much less persistent at 298 K and ultimately give the corresponding zwitterions in which $[BAr^F{}_4]^-$ coordinates and NBA is lost. The solid-state structures, as determined by X-ray crystallography, for all these $[BAr^F{}_4]^-$ adducts are reported. DFT calculations suggest that the molecular zwitterions within these structures are all significantly more stable than their corresponding σ-alkane cations, suggesting that the solid-state motif has a strong influence on their observed relative stabilities.

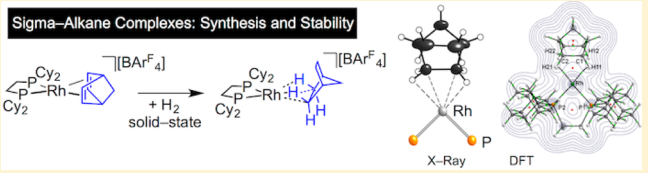

1. INTRODUCTION

The selective and atom-efficient functionalization of the C−H bonds in alkanes continues to be an important area of homogeneous catalysis. In particular, upgrading alkane feedstocks (such as methane and ethane) into commodity chemicals has the potential for enormous economic and societal impact.[1−3] Nevertheless, the controlled functionalization of these fossil-resource-derived hydrocarbons is difficult, and the development of selective transition-metal-catalyzed C−H activation processes that operate at low temperatures is one of the major challenges in the area of homogeneous catalysis.[4−8] A central problem in this endeavor is the fact that alkanes are poor nucleophiles, especially compared with arenes or olefins, where the π-systems encourage coordination to a metal center. In contrast, the C−H σ-bond is strong and non-polar, and steric interactions from the alkyl group also disfavor approach to a metal center. Alkanes are thus poor ligands, coordinating only weakly to metal centers to form σ-complexes with three-center, two-electron (3c-2e) M···H−C interactions,[9,10] typically with bond enthalpies of less than 15 kcal/mol.[11−13] This makes study of the subsequent C−H activation processes (whether by oxidative cleavage, electrophilic activation, or σ-CAM-assisted metathesis[10]) challenging, as intermediates are difficult to observe.[14]

Despite this, extensive investigations on the mechanism of C−H activation of alkanes using Pt(II)-catalyzed processes based upon the $[PtCl_4]^{2-}$ Shilov system have provided detailed insight into these processes.[15−22] These and other[23−26] mechanistic studies have provided compelling indirect evidence for the existence of σ M···H−C intermediates. Such transient intermediates (or closely related transition states) are also central to the catalytic functionalization of alkanes, for example, transition-metal-catalyzed alkane dehydrogenation,[5,27,28] alkane metathesis,[29] and alkane borylation,[30] as well as alkane activation processes catalyzed by post-transition metals,[31] and gas separation and alkane activation processes mediated by framework materials that also have coordinatively unsaturated metal sites.[32−34]

Direct evidence for σ-alkane complexes has come from a variety of spectroscopic and crystallographic techniques, slowly building over a period of 40 years.[14] Initial evidence for such species came from IR and UV/vis spectroscopy in CO-photodissociation experiments of group 6 and 8 carbonyls in methane matrices at very low temperatures (12 K).[35,36] More recently, fast spectroscopic techniques such as time-resolved infrared spectroscopy have been developed to study the coordination of alkanes with reactive metal carbonyls formed from photodissociation of a CO ligand.[13,37−40] These species are generally short-lived in solution, but the enhanced lifetime

Received: October 17, 2014
Published: December 15, 2014

DOI: 10.1021/ja510437p
J. Am. Chem. Soc. 2015, 137, 820−833

of some (hours), especially those of the 5d metals (Re and W), allows for their characterization at low temperatures (typically ca. 193 K) by NMR spectroscopy when *in situ* photodissociation techniques are used. For example photolysis of $Re(\eta^5\text{-}C_5H_4R)(CO)_3$ (R = H, ^{i}Pr) in alkanes (cyclopentane, pentane) led to the observation of σ-alkane complexes, exemplified by $Re(\eta^5\text{-}C_5H_5)(CO)_2$(cyclopentane), **A**, Chart 1.[41−43] In a similar manner, photolysis of $Mn(\eta^5\text{-}C_5H_5)(CO)_3$ in butane or propane forms the corresponding alkane complexes, e.g., **B**.[44] The supporting ligands can also be changed to other facially capping groups closely related to cyclopentadienyl.[45−47] These complexes are formed as mixtures with the starting materials and decompose on warming to room temperature. At low temperatures they have lifetimes from minutes to hours, and the products of decomposition are often the parent carbonyl, formed from recombination with photoejected CO. One way around this is to photo-eject N_2 from an appropriate precursor, for which a combination of being a significantly poorer nucleophile with a greater efficiency for photo-ejection compared with CO leads to higher *in situ* yields of the alkane products.[48]

Chart 1. Representative σ-Alkane Complexes Characterized by Low-Temperature NMR Spectroscopy

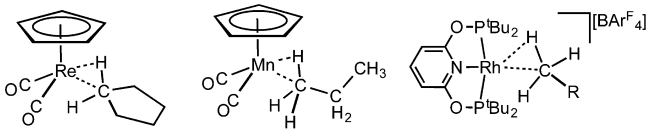

Recently, Brookhart and co-workers reported a different methodology for generating σ-alkane complexes at very low temperatures in solution, by protonation of a methyl or ethyl precursor Rh(PONOP)R (PONOP = 2,6-(^{t}Bu$_2$PO)$_2$C$_5$H$_3$N; R = Me, Et) using an acid with a non-coordinating counterion at temperatures between 193 and 123 K in $CDCl_2F$ solvent to form $[Rh(PONOP)(alkane)]^+$ in solution, e.g., **C**.[49−51] These complexes were long-enough lived at these low temperatures to allow full characterization by NMR spectroscopy, as the methane complex has a half-life of about 80 min at 186 K, although the ethane complex is significantly less stable. Both complexes decompose by irreversible coordination of solvent to form spectroscopically characterized solvent complexes, i.e., $[Rh(PONOP)(CDCl_2F)][BAr^F_4]$ (Ar^F = 3,5-$C_6H_3(CF_3)_2$).

The short lifetimes of all these alkane complexes even at very low temperatures, when coupled with their synthesis at often less than 100% efficiency, is a significant barrier to the generation of single-crystalline material suitable for study by X-ray diffraction, the "gold-standard" in coordination chemistry for structural elucidation. Until recently, only two examples had been reported in which a saturated hydrocarbon was located within bonding distance of a transition metal center in the solid state, allowing for an analysis of the molecular structure by single-crystal X-ray diffraction techniques (Chart 2). The first of these, **D**, shows a molecule of heptane interacting with an iron(II)−porphyrin complex,[52] although crystallographic disorder prevented the accurate analysis of the Fe−alkane interaction. The second example, **E**, involves cyclic alkane adducts of an unsaturated uranium(III) complex.[53] Both **D** and **E** result from incorporation of a solvent molecule within the coordination sphere of the metal, potentially assisted by host−guest effects in addition to any direct M···H−C bond interaction. Neither of these complexes is stable on solvation. Related structural diffraction studies come from the binding of light alkanes to iron centers in an extended metal−organic framework as characterized by powder neutron diffraction experiments, e.g., **F**.[32,33] Complexes in which there is a close intermolecular approach of an alkane to a group 1 cation (K^+) have also been reported, although these interactions are characterized as being weakly electrostatic and are further stabilized by interactions between the alkane and a hydrophobic ligand pocket.[54]

Chart 2. Previously Reported Examples of σ-Alkane Complexes Characterized in the Solid State by Diffraction Techniques

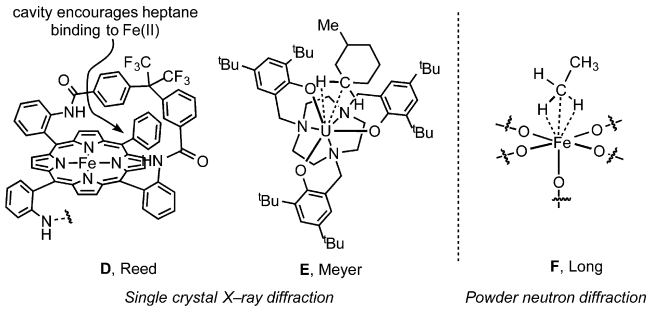

Recognizing that a significant barrier to characterizing σ-alkane complexes in the solid state by X-ray diffraction is their instability in solution on the time scales and at the temperatures required for the production of single crystals, we recently reported the use of solventless conditions,[55] i.e., gas/solid reactivity, to synthesize a σ-alkane complex directly in the solid state, Scheme 1. In this crystal-to-crystal transformation,[56−62] a crystalline norbornadiene (NBD) Rh precursor, [**1-NBD**]-[$\mathbf{BAr^F_4}$], was treated with dihydrogen, resulting in addition of H_2 to the diene to form directly a saturated norbornane (NBA) fragment bound to the Rh(I) center through two 3c-2e Rh···H−C interactions, [**1-NBA**][$\mathbf{BAr^F_4}$].[59] Hydrogenation of ring-strained NBD in $[Rh(L)_2(NBD)]^+$ (L = phosphine) was reported by Schrock and Osborn in 1976 using solution methods,[63−65] and has since been studied in some detail, in particular for the asymmetric hydrogenation of alkenes.[66,67] Of course, when the reaction is performed in solvent, the alkane generated is simply lost from the metal's coordination sphere, either as the desired product of the reaction or in generating

Scheme 1. Synthesis of a Rh(I) σ-Alkane Complex by a Solid/Gas Single-Crystal to Single-Crystal Methodology (SS = Solid State)

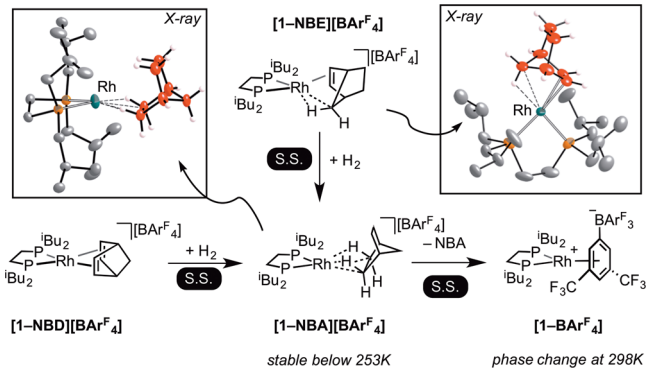

DOI: 10.1021/ja510437p
J. Am. Chem. Soc. 2015, 137, 820−833

the active catalyst. In the solid state, this process is attenuated to the extent that [**1-NBA**][BAr^F_4] has a lifetime that allows for its characterization by both single-crystal X-ray diffraction (at 150 K) and $^{31}P\{^1H\}$ solid-state NMR spectroscopy at 253 K. Above 253 K, the thermodynamic product forms in which the $[BAr^F_4]^-$ anion has replaced the alkane (NBA) at the metal center to form a zwitterionic product, [**1-**BAr^F_4]. At this point crystallinity is lost, due to both the expulsion of NBA from the lattice and the large change in lattice volume associated with this coordination of the anion: [**1-NBD**][BAr^F_4], 5957.6(2) Å^3; [**1-NBA**][BAr^F_4], 6044.1(3) Å^3; and [**1-**BAr^F_4], 5429.1(3) Å^3. [**1-NBA**][BAr^F_4] can also be prepared from the corresponding norbornene precursor, [**1-NBE**][BAr^F_4], in a solid/gas reaction that does not lose crystallinity. That [**1-NBE**][BAr^F_4] is also an intermediate in the overall reaction is shown by addition of D_2 to [**1-NBD**][BAr^F_4], which results in the formation of *exo*/*endo* d_4-NBA, and addition of D_2 to [**1-NBE**][BAr^F_4], which gives *exo* d_2-NBA.[65,66] Combined, these experiments demonstrate a remarkable ability for the organic fragment to undergo reorganization in the solid state. We speculated that [**1-NBA**][BAr^F_4] had a lifetime in the solid state that is sufficient for X-ray crystallographic characterization because the $[BAr^F_4]^-$ anions provide a well-defined octahedral cavity in the lattice that both traps the alkane and accommodates the structural changes associated with alkene hydrogenation.

In this contribution we now report, using similar methodology, an exploration into the effects of changing the chelating phosphine backbone length (ethylene and propylene), the identity of the phosphine substituent (Cy, ^{i}Pr, O^{i}Pr), and the anion on the resulting stability of the alkane complex. As part of this we report the remarkable example of an indefinitely (months) room-temperature-stable transition metal σ-alkane complex, alongside its characterization by solid-state NMR spectroscopy and an assessment of its electronic structure by computational methods.

2. RESULTS AND DISCUSSION

2.1. Changing the Anion. Recently we reported that changing the anion from $[BAr^F_4]^-$ to the more strongly coordinating, but pseudo-structural, $[BAr^{Cl}_4]^-$ anion [Ar^{Cl} = 3,5-$C_6H_3Cl_2$][68] resulted in a NBD complex that underwent solid/gas reactivity with H_2 to immediately form the arene-coordinated zwitterion analogous to [**1-**BAr^F_4] without the intermediate alkane complex being observed.[69] Changing the anion to other, least-coordinating anions such as $[B(C_6F_5)_4]^-$, $[Al(OC(CF_3)_3)_4]^-$ or $[Al(OCH(CF_3)_2)_4]^-$[70] led to intractable oils for the NBD salts that were resistant to recrystallization. Thus, they were not explored further here.

2.2. [Rh(Cy$_2$PCH$_2$CH$_2$PCy$_2$)]$^+$. *2.2.1. Synthesis and Characterization of [Rh(Cy$_2$PCH$_2$CH$_2$PCy$_2$)(NBD)][BAr$^F_4$], [2-NBD][BAr$^F_4$], a Precursor to a σ-Alkane Complex.* The required precursor for the synthesis of σ-alkane complexes using our methodology is a Rh−NBD adduct. We have found that the best route for the synthesis of [Rh(Cy$_2$PCH$_2$CH$_2$PCy$_2$)(NBD)][BAr^F_4], [**2-NBD**][BAr^F_4], was via a corresponding fluorobenzene adduct, [**2-**C_6H_5F][BAr^F_4], which in turn was prepared from hydrogenation of a COD precursor in C_6H_5F solvent, Scheme 2. [**2-NBD**][BAr^F_4] could be prepared analytically pure and recrystallized from CH_2Cl_2/pentane solvent mixture to give reasonably sized (e.g., 0.5 × 0.5 × 0.1 mm) blood-red single crystals in 59% yield. The resulting single-crystal X-ray structure of [**2-NBD**][BAr^F_4] is shown in Figure 1.

Scheme 2. Synthesis of [2-NBD][BAr^F_4]

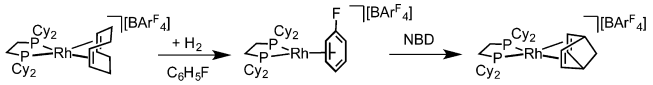

[2–COD][BAr^F_4] [2–C_6H_5F][BAr^F_4] [2–NBD][BAr^F_4]

The cation in [**2-NBD**][BAr^F_4] shows unremarkable structural metrics, being closely related to [**1-NBD**][BAr^F_4].[59] Noteworthy for later comparison with the σ-alkane complex [**2-NBA**][BAr^F_4] are the alkene C−C distances [C1−C2, 1.385(10); C4−C5, 1.374(10) Å] and the Rh−P distances [Rh1−P1, 2.2940(13); Rh1−P2, 2.2845(13) Å]. There is no crystallographically imposed symmetry to the cation, and no disorder present. The $[BAr^F_4]^-$ anions in the lattice are organized so that each cation is surrounded by six anions in a close to octahedral cage arrangement (Figure 1B and Supporting Information, Figure S1). The cross-cage B···B distances are 17.26(2), 19.23(1), and 19.832(8) Å, while the unit cell volume is 3287.04(13) Å^3 (Z = 2). One of the $[BAr^F_4]^-$ anions is orientated so that two of its aryl groups enfold the NBD fragment (Figure 1C). These metrics and the gross motif are very similar to those reported for [**1-NBD**][BAr^F_4] [17.06(1)−18.779(1) Å; 5957.62(19) Å^3, Z = 4].[59] This orientation of the aryl groups on the anion brings the bridge methylene protons on C7 in close approach to the center of the arene rings: H···centroid = 2.502 and 2.548 Å.

Solution NMR spectroscopic data for [**2-NBD**][BAr^F_4] are in full accord with the formulation. Magic angle spinning solid-state $^{31}P\{^1H\}$ and $^{13}C\{^1H\}$ NMR spectroscopic data (SSNMR) are also fully consistent with the solid-state structure. Two broad and closely spaced signals at ca. δ 76, both showing coupling to ^{103}Rh [J(RhP) ≈ 123, 122 Hz] are observed in the $^{31}P\{^1H\}$ SSNMR spectrum (Figure 2A), in line with crystallographic non-equivalence of the phosphine groups. In the $^{13}C\{^1H\}$ NMR spectrum (Figure 3A), in addition to signals assigned to $[BAr^F_4]^-$ aryl groups (δ 164−116) and alkyl phosphine groups (δ 40−20), four signals are observed at δ 91, 82, 70 (br), and 55.[71] Aided by DFT chemical-shift calculations, these signals are assigned to C═C (C1, C4), C═C (C2, C5), C(7), and C(3,6), respectively (see Supporting Information, Figures S2 and S11). The slight broadening of the bridge methylene group (C7) in comparison with the other signals of the NBD ligand is consistent with strong homonuclear coupling between the geminal protons.[72]

2.2.2. Synthesis and Characterization of the σ-Alkane Complex [Rh(Cy$_2$PCH$_2$CH$_2$PCy$_2$)(NBA)][BAr$^F_4$], [2-NBA][BAr$^F_4$]. With complex [**2-NBD**][BAr^F_4] in hand, we then proceeded to study its solid/gas reactivity with H_2. Hydrogenation of a single-crystalline sample led to the quantitative and rapid formation of the σ-alkane complex [**2-NBA**][BAr^F_4], [Rh(Cy$_2$PCH$_2$CH$_2$PCy$_2$)(η^2,η^2-NBA)][BAr^F_4] (Scheme 3). There is little color change from the original starting material, and although the crystals go opaque they retain crystallinity. A $^{31}P\{^1H\}$ SSNMR of the reaction soon after H_2 addition (10 min) shows that no [**2-NBD**][BAr^F_4] remains and a single phosphorus-containing product is formed, that shows two closely spaced doublet resonances at ca. δ 110 [J(RhP) ≈ 207 and 216 Hz] (Figure 2B). Such a downfield shift and increase in the ^{103}Rh−^{31}P coupling constant is consistent with the formation of a σ-alkane complex, as reported for [**1-NBA**][BAr^F_4].[59] The $^{13}C\{^1H\}$ SSNMR spectrum demonstrates the disappearance of signals due to NBD between δ 100 and 55

DOI: 10.1021/ja510437p
J. Am. Chem. Soc. 2015, 137, 820−833

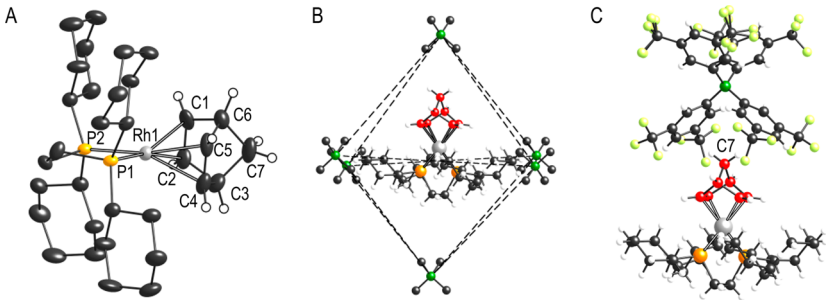

Figure 1. (A) Solid-state structure of the cationic portion of complex [**2-NBD**][**BAr$^F_4$**]. Displacement ellipsoids are shown at the 50% probability level. Selected bond lengths (Å) and angles (deg): Rh1−P1, 2.2940(13); Rh1−P2, 2.2845(13); Rh1−C1, 2.214(6); Rh1−C2, 2.217(5); Rh1−C4, 2.211(6); Rh1−C5, 2.225(6); C1−C2, 1.385(10); C4−C5, 1.374(10); P1−Rh1−P2, 85.04(5). (B) Packing diagram with aryl groups on the anions removed. B···B cross-cage distances = 17.26(2), 19.23(1), 19.832(8) Å. For a related structure showing the full disposition of the aryl groups, see Figure 5A. (C) Relationship between [**2-NBD**]$^+$ and one of the [BAr$^F_4$]$^-$ anions. Shortest distances between the H-atoms on C7 and the centroids of the two aryl rings = 2.502, 2.548 Å.

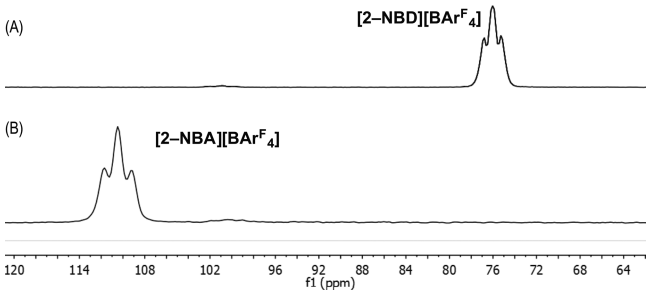

Figure 2. $^{31}P\{^1H\}$ SSNMR spectra of H_2 addition to powdered crystalline [**2-NBD**][**BAr$^F_4$**]. (A) [**2-NBD**][**BAr$^F_4$**], 298 K. (B) H_2 addition (4 atm), 2 h, 298 K to form [**2-NBA**][**BAr$^F_4$**].

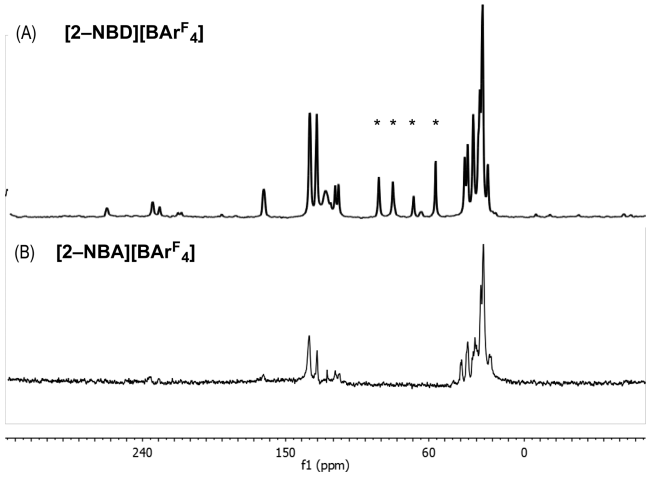

Figure 3. $^{13}C\{^1H\}$ SSNMR (10 kHz) spectra of H_2 addition to powdered crystalline [**2-NBD**][**BAr$^F_4$**]. (**A**) [**2-NBD**][**BAr$^F_4$**], 298 K. * indicates signals due to the NBD group, see text. (B) H_2 addition (4 atm), 2 h, 298 K to form [**2-NBA**][**BAr$^F_4$**]. Spinning side bands are not marked.

Scheme 3. Synthesis of [2-NBA][BAr$^F_4$]

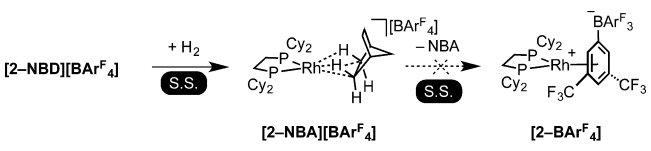

(Figure 3B), while DFT chemical shift calculations suggest that signals due to the NBA ligand are located between δ 21 and 45, in the region also associated with the cyclohexyl groups on the phosphine ligand. No signals that could be attributed to a coordinated [BAr$^F_4$]$^-$ aryl group were observed (i.e., δ 90–100),[59,73] discounting the formation of zwitterionic [**2-BAr$^F_4$**] as a product. Crystalline and powdered samples of [**2-NBA**][**BAr$^F_4$**] are stable at 298 K for a significant period of time. For example after 16 h acquisition the SSNMR spectra show little change to the $^{31}P\{^1H\}$ NMR spectra, while crystalline material is stable under argon for over four months as determined by single-crystal X-ray diffraction. This remarkable stability contrasts with that of [**1-NBA**][**BAr$^F_4$**] which although stable at low temperature, 253 K, on warming to room temperature proceeds to form the [BAr$^F_4$]$^-$-coordinated zwitterion [**1-BAr$^F_4$**] and free NBA within hours.[59] This means that for **2** hydrogenation of the NBD precursor to form the σ-alkane complex as the only product has no real temporal constraint; unlike for [**1-NBD**][**BAr$^F_4$**] in which rapid transfer at low temperature of freshly hydrogenated single crystals to the X-ray diffractomer is required. It should be noted that both previously reported neutral complexes **D**[52] and **E**,[53] that show evidence for an alkane ligand in close approach to the metal center, have not been reported to proceed with further reactivity in the solid state.

The solid-state structure, as determined by single-crystal X-ray diffraction at 150 K, of [**2-NBA**][**BAr$^F_4$**], is shown in Figure 4, which clearly shows a saturated NBA fragment interacting with the Rh center through two 3c-2e Rh···H−C interactions. Figure 5 shows that the relationship in the lattice between the [BAr$^F_4$]$^-$ anions and the cation is very similar to [**2-NBD**][**BAr$^F_4$**]. Interestingly this single-crystal to single-crystal transformation involves a change in space group upon hydrogenation, from $P\bar{1}$ (Z = 2) in the NBD adduct to $P2_1/n$ (Z = 4) in the alkane adduct. Similar changes in space group during a single-crystal to single-crystal transformation have recently been reported by Balch and co-workers for the α- and β-forms of $Au_2(\mu\text{-dppe})_2I_2\cdot 2OCMe_2$ ($P2_1/c$ and $P\bar{1}$, respectively).[74] Complex [**2-NBA**][**BAr$^F_4$**] shows no disorder in the solid state for the cation, and the high quality of the diffraction data resulted in a very good structural refinement that even allowed for the location and free refinement of the hydrogen atoms. This is the first time this has been achieved in such a motif by single-crystal X-ray diffraction, as disorder (i.e., **D**[52] or [**1-NBA**][**BAr$^F_4$**][59]) or placement in calculated positions (**E**[53])

DOI: 10.1021/ja510437p
J. Am. Chem. Soc. 2015, 137, 820–833

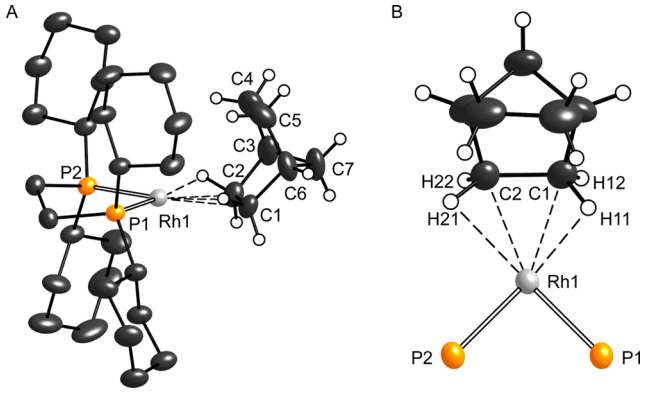

Figure 4. (A) Solid-state structure of the cationic portion of complex [**2-NBA**][**BAr$^F_4$**]. Displacement ellipsoids are shown at the 50% probability level. (B) Alternate view, with phosphine alkyl groups removed and showing selected H-atom labeling on the NBA fragment. Selected bond lengths (Å) and angles (deg): Rh1−P1, 2.1932(7); Rh1−P2, 2.1950(7); Rh1−C1, 2.389(3); Rh1−C2, 2.400(3); Rh1−H11, 1.95(4); Rh1−H21, 1.93(4); C1−C2, 1.552(4); C4−C5, 1.546(7); C1−H11, 0.99(4); C1−H12, 0.97(4); C2−H21, 1.02(4); C2−H22, 0.97(4); P1−Rh1−C1, 118.56(8); C1−Rh1−C2, 37.8(1); P2−Rh1−C2, 118.17(8); P1−Rh1−P2, 85.19(3); C2−C1−H12, 110(2); C2−C1−H11, 122(2); C1−C2−H22, 112(2); C1−C2−H21, 120(2); sum of angles around Rh1, 359.7.

have precluded such analysis. In framework materials such as **F** (Chart 2) D-atoms have been located by powder neutron diffraction experiments.[32]

In [**2-NBA**][**BAr$^F_4$**] the NBA ligand binds to the {Rh(L$_2$)}$^+$ fragment through two C−H σ interactions, resulting in a Rh(I), square planar, d^8 metal center coordination motif. The key Rh−C1 and Rh−C2 distances are 2.389(3) and 2.400(3) Å, respectively, and so lie well within the combined van der Waals radii of Rh and C−H (3.44 Å).[75] These distances are also at the low end of the range reported for intramolecular Rh−C distances in representative Rh(I)-agostic complexes (2.4−2.6 Å).[76−80] DFT calculations (vide infra) give an average computed Rh−C distance of 2.438 Å, in good agreement with experiment, and also similar to values calculated for [Rh(PONOP)L]$^+$ complexes (L = CH$_4$, 2.380 Å; L = H$_3$CCH$_3$, 2.431 Å).[49,51] The C1−C2 [1.552(4) Å] and C4−C5 [1.546(7) Å] distances are clearly single bonds, having lengthened significantly on hydrogenation of the [**2-NBD**][**BAr$^F_4$**] precursor. These similar C1−C2 and C4−C5 distances suggest no Rh···C1−C2 agostic interaction is present, despite the Rh−C1/C2 distances falling within the range observed in such complexes.[81−83] Calculations (*vide infra*) also confirm the absence of any such interactions.

Although H atoms were located in the difference map, the limited accuracy possible with with X-ray crystallography means any metrical differences involving H atoms are not statistically significant, with C−H distances ranging from 0.97(4) to 1.02(4) Å. However, in combination with DFT calculations, some important features can be highlighted. In particular a small lengthening of the C−H bonds when bound to the Rh center is seen, with the calculated C1−H11 and C2−H21 distances averaging 1.157 Å compared to 1.101 Å for the spectator C1−H12 and C2−H22 bonds. A widening of the C−C−H angles when the C−H bond is interacting with the Rh center is also apparent [X-ray: C1−C2−H21 120(2)°, C1−C2−H22 112(2)°; DFT: C1−C2−H21 118.7°, C1−C2−H22 111.2°]. The average DFT-computed Rh−H11/H21 distance is 1.901 Å and both experiment and calculation suggest the Rh···H−C interactions are relatively weak, based on a ca. 0.1 Å shortening of the Rh−P distances *trans* to the alkane in [**2-NBA**][**BAr$^F_4$**] compared to those *trans* to the alkene in [**2-NBD**][**BAr$^F_4$**] [X-ray: e.g., 2.1932(2) versus 2.2845(13) Å; DFT: 2.251 versus 2.360 Å, respectively]. These Rh···H−C interactions will be quantified in the Computational Section.

The Rh−C1/C2 distances in [**2-NBA**][**BAr$^F_4$**] are slightly shorter than those reported in the disordered structure of [**1-NBA**][**BAr$^F_4$**] [2.480(1) and 2.494(10)].[59] By comparison the M−C distances in complexes exemplified by **D** [Fe···C 2.5−2.8 Å for a highly disordered structure],[52] **E** [U···C 3.731(8)−3.864(7) Å],[53] and **F** [Fe···C distances ∼3 Å][32] are all considerably longer than for [**2-NBA**][**BAr$^F_4$**] even before the appropriate covalent radii have been taken into account,[84] suggesting a more significant interaction between the alkane and the Rh center in [**2-NBA**][**BAr$^F_4$**]. With its two σ, chelating, Rh···H−C interactions, complex [**2-NBA**][**BAr$^F_4$**] is also related to crystallographically characterized σ-bis-silane,[85] σ-dihydrogen,[86] adjacent CH/BH agostic,[87] and σ-diborane(4) complexes.[88,89] There is also a structural similarity with the intramolecular agostic norbornyl complex [Pt(C$_7$H$_{11}$)-(^{t}Bu$_2$PCH$_2$CH$_2$P^{t}Bu$_2$)][BPh$_4$] reported by Spencer, which is formed by protonation of a neutral NBE complex.[90] Intermolecular Rh···H−C$_{aryl}$ interactions have recently been reported in the solid state in a Rh(PBP) boryl pincer complex [Rh···C 2.766(2) Å], although these are significantly longer than found in [**2-NBA**][**BAr$^F_4$**].[91]

The [BAr$^F_4$]$^-$ anions in [**2-NBA**][**BAr$^F_4$**] retain the same pseudo octahedral motif as seen in the extended structure of [**2-NBD**][**BAr$^F_4$**] (Figure 5A, B), and the same relationship

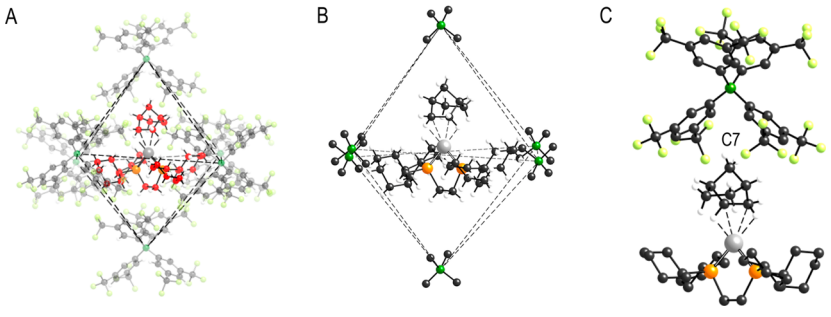

Figure 5. (A) Packing diagram showing the relationship of the six closest [BAr$^F_4$]$^-$ anions to the [**2-NBA**]$^+$. (B) Packing diagram with aryl groups on the anions removed. B···B cross-cage distances = 17.975(4), 19.042(4), 19.560(5) Å. (C) Relationship between [**2-NBA**]$^+$ and one of the [BAr$^F_4$]$^-$ anions. Closest distance between the methylene protons on C7 and the centroids of the aryl rings on the anion = 2.98, 3.18 Å.

DOI: 10.1021/ja510437p
J. Am. Chem. Soc. 2015, 137, 820−833

between a single anion and cation is also retained (Figure 5C), with the NBA ligand sitting in a cleft between two of the anion aryl rings. Similar to [**2-NBA**][**BAr$^F_4$**] there is also a close approach of one of the bridge NBA methylene protons on C7 to the center of two of the anion aryl groups [2.98 and 3.18 Å]. The B···B cross cage distances have also not changed significantly between the two structures, while the unit cell volume has changed by only +1.8% (normalized Z): 6691.62(9) (Z = 4) versus 3287.04(13) Å^3 (Z = 2), respectively. This cavity described by the anions allows for the movement of the organic fragment in going from NBD to NBA in the final product in which a transformation from two bound alkenes to one bidentate σ-bis-alkane fragment occurs. We suggest that the hydrogenation proceeds via an NBE intermediate,[92] possibly related to that reported for complex [**1-NBD**][**BAr$^F_4$**].[59] Within this cavity there are a number of weak C−H···F−C hydrogen bonds[93] between the [BAr$^F_4$]$^-$ CF_3 groups and the C−H on the cyclohexyl and NBA fragments, ranging between 2.4 and 2.8 Å (Supporting Information, Figure S3). Similar interactions are also present in [**2-NBD**][**BAr$^F_4$**]. Finally, comparison of the overall structures of the cations in [**2-NBA**][**BAr$^F_4$**] and [**2-NBD**]-[**BAr$^F_4$**] shows that there has been very little change in the chelating phosphine ligand upon hydrogenation (Figure S4), with only a slight difference in the orientation of one of the cyclohexyl groups with regard to Rh−P−C−C torsion angle.

2.2.3. Attempted Characterization of [2-NBA][BAr$^F_4$] in solution. σ-Rh···HC interactions in complexes such as **C** (Chart 1)[49,51] have been successfully observed in solution at very low temperature (193 to 130 K) using a Freon ($CDCl_2F$) solvent.[94] We have previously reported that [**1-NBA**][**BAr$^F_4$**] produced via the solid-state route, when dissolved in $CDCl_2F$, affords a major product at low temperature (−110 °C) that is not the bound alkane complex (free NBA was observed), which we tentatively described as a solvent adduct of [Rh-(^{i}Bu$_2$PCH$_2$CH$_2$P^{i}Bu$_2$)]$^+$ or a complex with agostic interactions. Warming to −20 °C resulted in the formation of [**1-BAr$^F_4$**].[59] Thus, the alkane is only weakly bound at best in solution, being rapidly displaced by solvent.

Dissolving [**2-NBA**][**BAr$^F_4$**] in $CDCl_2F$ at 133 K resulted in a $^{31}P\{^1H\}$ NMR spectrum that showed two environments, both as doublets, at δ 94.6 [J(RhP) = 195 Hz] and 91.0 [J(RhP) = 208 Hz]. In the ^{1}H NMR spectrum signals due to free NBA were observed, and there were no signals observed at high field characteristic of Rh···H−C interactions. Multiple environments were observed in the arene region, while in the ^{19}F NMR spectrum 8 different environments of equal area are observed. These data suggest that the zwitterion [**2-BAr$^F_4$**], [Rh-(Cy$_2$PCH$_2$CH$_2$PCy$_2$){(η-C$_6$H$_3$(CF$_3$)$_2$)BAr$^F_3$)], has been formed on dissolution (see section 2.2.5), in contrast to a solvent complex suggested for **1**, and at very low temperature libration of the [RhL$_2$]$^+$ fragment on the arene ring and rotation around the B−C bond of the bound arene is halted. Warming to 173 K results in a much simpler set of spectra that shows a single ^{31}P environment, only two environments in the ^{19}F NMR spectrum in a ratio of 6:18, and a ^{1}H NMR spectrum in the aromatic region that shows only four environments in the relative ratio 3:6:2:1. These data are very much like those for independently prepared [**2-BAr$^F_4$**] in CD_2Cl_2 solution at 193 K (vide infra). We thus suggest that, on warming, libration of the metal fragment and rotation around the B−C bond occur. Minor decomposition products, indicated by free [BAr$^F_4$]$^-$, also grow in with increasing time and temperature.

2.2.4. Characterization of the Rh···H−C σ Interaction by SSNMR Spectroscopy. The ready dissociation of the NBA alkane ligand when dissolved in solution (even at very low temperatures) prevents the observation of the Rh···HC interaction by solution NMR techniques. Although ^{1}H SSNMR spectroscopy might thus then appear to be the ideal technique, the investigation of hydrogen interacting with metal centers by ^{1}H solid-state NMR spectroscopy can be problematic due to the small chemical shift range (~20 ppm) and large line widths that arise from strong proton background signals from supporting ligands and strong homonuclear proton−proton dipolar interactions.[95] Perhaps for this reason σ complexes (e.g., dihydrogen complexes) have not been extensively studied using SSNMR techniques, although isotopic substitution of H for D avoids many of the issues associated with ^{1}H SSNMR.[92,96,97] However, a recent report describes the use of ^{1}H wPMLG (window phase-modulated Lee−Goldburg) ^{1}H−^{29}Si dipolar HECTOR SSNMR experiments to directly observe agostic Ru···H−Si interactions in the solid state,[98] while agostic interactions on surface-supported organometallics have been indirectly characterized using 2D J-resolved techniques.[99]

For [**2-NBA**][**BAr$^F_4$**] we have used indirect detection of the ^{1}H NMR spectrum by utilizing a frequency-switched Lee−Goldburg (FSLG) ^{1}H−^{13}C HECTOR SSNMR experiment. The results of this are shown in Figure 6, and analysis is aided

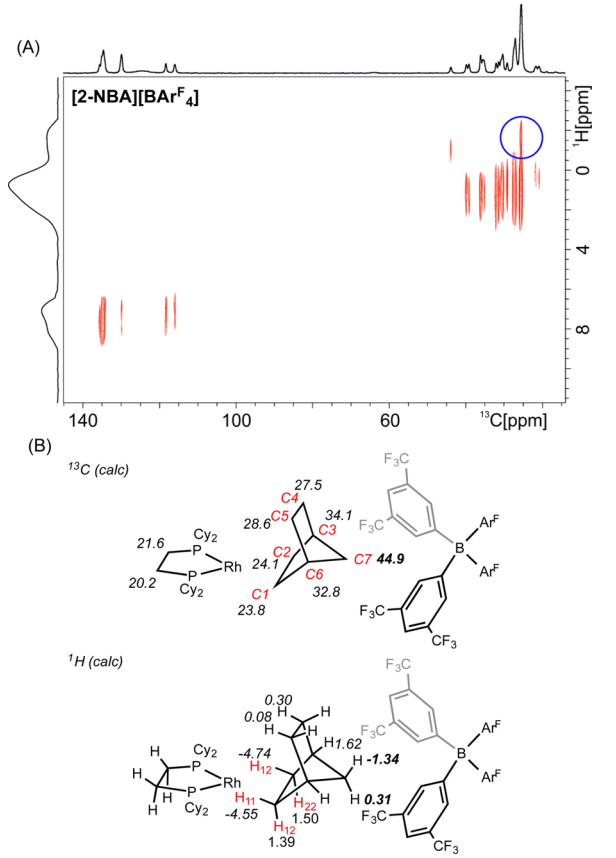

Figure 6. (A) ^{1}H/^{13}C frequency-switched Lee−Goldburg HECTOR SSNMR (10 kHz) of [**2−NBA**][**BAr$^F_4$**]. Circled cross−peaks show peaks assigned to Rh···H−C. The F1-axis is a projection of the ^{1}H NMR spectrum. (B) ^{13}C and ^{1}H calculated chemical shifts based on the isolated [**2-NBA**][**BAr$^F_4$**] ion-pair (at the M06(SDD/6-31G**)//BP86(SDD/6-31g**) level).

DOI: 10.1021/ja510437p
J. Am. Chem. Soc. 2015, 137, 820−833

by DFT-calculated ^{13}C and ^{1}H chemical shifts. It is apparent that there are three distinct regions in the projected ^{1}H NMR spectrum: a set of signals grouped around δ 8 assigned to the $[BAr^{F}_{4}]^{-}$ anion, one centered around δ 1 assigned to the Cy/NBA groups and a broad signal ca. δ −2, in the chemical shift region associated with σ interactions. The first two regions also correlate as expected to the appropriate chemical shift regions of the ^{13}C NMR spectrum. For the high field region of the ^{1}H NMR projection the broad signal centered at ca. δ −2 correlates to a signal at δ 25 in the $^{13}C\{^{1}H\}$ NMR spectrum; and calculations predict the C1 and C2 contact carbons (Figure 6B) resonate in this region [computed values at the M06/SDD level of theory: $\delta(^{13}C)$ 24.1 and 23.8; $\delta(^{1}H)$ −4.6 and −4.7 for the [**2-NBA**][**BAr$^{F}_{4}$**] isolated ion pair using the heavy atom positions derived from the X-ray structure with optimized H-atom positions]. For complexes such as **C** the σ Rh···H_2C interactions are observed at ca. δ −0.8 in the ^{1}H NMR solution spectrum, and also show a small (ca. 6 Hz) coupling to ^{103}Rh.[49,51] Such a small coupling would not be resolved for [**2-NBA**][**BAr$^{F}_{4}$**] using solid-state NMR experiments. Interestingly, the $[Rh(PONOP)(alkane)]^{+}$ complexes show very high field shifted signals for the contact carbon atoms (e.g., δ −41.7 for **C**,[49,51] compared to δ −4.33 for free CH_4[100]). Such dramatically high-field shifted signals are not observed for [**2-NBA**][**BAr$^{F}_{4}$**], as confirmed by measuring the spectrum down to −80 ppm. Instead the computed ^{13}C chemical shifts of [**2-NBA**][**BAr$^{F}_{4}$**] demonstrate only a small high-field shift between the coordinated alkane carbons (C1/C2: ca. δ 24) and the non-coordinated sites (C4/C5: ca. δ 28).[101] In support of this small change in chemical shift, closely related *agostic* complexes such as $[Pt(C_7H_{11})\{^{t}Bu_2P(CH_2)_3P^{t}Bu_2\}][BPh_4]$[90] or $[Rh(P^{i}Bu_3)(\kappa^3\text{-}P^{t}Bu_2CH_2CH_2CH{=}CH_2)][BAr^{F}_{4}]$[79] show the Rh···C(agostic) groups at very similar chemical shifts to that observed for [**2-NBA**][**BAr$^{F}_{4}$**] (i.e., δ 30.0 and 24.8, respectively). A cross peak between a signal in the ^{1}H NMR projection at approximately δ −1 and $\delta(^{13}C)$ 43.5 is assigned to the bridge CH_2 groups on the NBA that sit in a cleft between two $[BAr^{F}_{4}]^{-}$ aryl groups (i.e., C7, Figure 5C). Such an orientation might be expected to promote ring-current shielding, accounting for the relatively high field chemical shift of the CH_2 protons. This analysis is given further weight by the observation of a similar cross peak in the $^{1}H-^{13}C$ HECTOR SSNMR spectrum of [**2-NBD**][**BAr$^{F}_{4}$**] (Figure S2), between a high field signal in the ^{1}H NMR projection (δ −0.52) and the signal assigned to the bridge CH_2 group (δ 70), which also has a similar relative orientation of aryl and methylene groups in the solid state to that found in [**2-NBA**][**BAr$^{F}_{4}$**] (Figure 1C). Similar high-field, ring-current effect, chemical shifts have been observed by ^{1}H SSNMR techniques in host−guest complexes where the distances between the shifted proton and the centroid of an arene is ∼2.6 Å, similar to those found here.[102,103] Moreover, these relative shifts are recreated in the calculated ^{1}H and ^{13}C chemical shifts for the isolated ion pairs in both [**2-NBD**][**BAr$^{F}_{4}$**] and [**2-NBA**][**BAr$^{F}_{4}$**], and equally importantly these are only reproduced when the anion is present (Figure 6B and Supporting Information, Figure S11). In the ^{1}H NMR projection of [**2-NBD**][**BAr$^{F}_{4}$**] there are also no high-field signals observed at ca. δ −2. Taken collectively these data, alongside the fact that the same sample batch was used for both X-ray diffraction analysis, solid-state NMR studies and microanalysis, suggests that the highest-field signals in the ^{1}H NMR projection of the $^{1}H-^{13}C$ HECTOR SSNMR spectrum can be assigned to the Rh···H−C environments. This identification of intermolecular σ M···H−C interaction involving an alkane complex using solid-state NMR spectroscopy complements recently reported M···H−Si examples.[98]

2.2.5. Synthesis and Characterization of [2-BAr$^{F}_{4}$], [Rh(Cy$_2$PCH$_2$CH$_2$PCy$_2$){(η-C$_6$H$_3$(CF$_3$)$_2$)BAr$^{F}_{3}$}]. The stability of [**2-NBA**][**BAr$^{F}_{4}$**] compared with [**1-NBA**][**BAr$^{F}_{4}$**] is remarkable, with the former being stable for months at room temperature (under an inert atmosphere) while the latter rapidly (hours) forms [**1-BAr$^{F}_{4}$**] under the same conditions. We were thus interested to see if [**2-BAr$^{F}_{4}$**] could be isolated, as its lack of formation from [**2-NBA**][**BAr$^{F}_{4}$**] in the solid state might suggest otherwise. In fact it can be synthesized using solution techniques, showing that it is an accessible species, but only in very low isolated yield. Dissolution of [**2-NBA**][**BAr$^{F}_{4}$**] in CH_2Cl_2 at 298 K, immediate filtration to remove significant amounts of gray decomposition products, extraction into pentane and storage at 253 K resulted in a very small number of orange crystals of [**2-BAr$^{F}_{4}$**] (eq 1). The solid-state structure

$$[\textbf{2-NBA}][\textbf{BAr}^{F}_{4}] \xrightarrow[\text{recrystallize from pentane}]{CH_2Cl_2} [\textbf{2-BAr}^{F}_{4}] \quad (1)$$

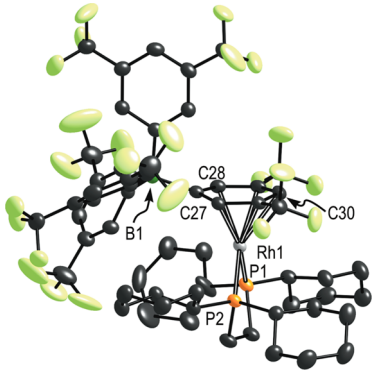

Figure 7. Solid-state structure of [**2-BAr$^{F}_{4}$**]. Displacement ellipsoids are shown at the 50% probability level. Selected bond lengths (Å) and angles (deg): Rh1−P1, 2.2720(6); Rh1−P2, 2.2638(6); Rh1−C27, 2.472(2); Rh1−C28, 2.357(2); Rh1−C30, 2.370(2); Rh1−C32, 2.270(2); P1−Rh1−P2, 84.15(2).

of [**2-BAr$^{F}_{4}$**] is shown in Figure 7. Structural metrics are very similar to those reported for [**1-BAr$^{F}_{4}$**][59] (Table S1) with five of Rh−C(aryl) distances spanning the range 2.270(2)−2.357(2) Å. There is one longer Rh−C(aryl) distance, that to the ipso carbon C27 [Rh−C27 2.472(2) Å] that suggests an η^5 coordination motif.[104] These are reproduced in the structures computed by DFT for [**2-BAr$^{F}_{4}$**] (see Supporting Information, Figure S9, Table S3). Solution NMR spectroscopic characterization was performed by dissolving [**2-NBA**][**BAr$^{F}_{4}$**] in cold CD_2Cl_2 (197 K) and transfer to a pre-cooled spectrometer. However, even at this temperature decomposition was observed to unidentified species that also liberated free anion. Nevertheless the low temperature ^{1}H and ^{19}F solution NMR data in CD_2Cl_2 are consistent with the formation of a zwitterionic complex, and are fully consistent with the formulation shown in the solid state as well as previously reported examples of $[BAr^{F}_{4}]^{-}$ coordinated to a metal center.[59,73] For example a single ^{31}P environment is observed at δ 91.5 [J(RhP) = 201 Hz] in the $^{31}P\{^{1}H\}$ NMR spectrum;

DOI: 10.1021/ja510437p
J. Am. Chem. Soc. 2015, 137, 820−833

signals due to a bound arene are observed in the ^{1}H NMR spectrum at δ 7.24 (1 H) and δ 7.08 (2 H), while the non-bound rings are equivalent (due to rotation around the B1−C27 bond) and show as two environments in a 3:6 ratio. Two resonances in a relative ratio of 6:18 are observed in the ^{19}F NMR spectrum. Thus, [**2-BAr$^F_4$**] is an accessible species in solution (albeit being very reactive in CD_2Cl_2), perhaps suggesting that its lack of formation from [**2-NBA**][**BAr$^F_4$**] is unlikely to be thermodynamic in origin, but more likely kinetic factors in the solid state are important. However, there is the caveat that the solution and solid-state thermodynamics might differ due the local environment provided by the lattice. Whatever the reasons behind this stability, clearly the Cy groups in the phosphine have an influence in this, as this is the only structural feature that has changed between **1** and **2**.

2.3. [Rh(^{i}Pr$_2$PCH$_2$CH$_2$P^{i}Pr$_2$)]$^+$. To further probe the influence of the groups on the phosphine, the complex [Rh(^{i}Pr$_2$PCH$_2$CH$_2$P^{i}Pr$_2$)(NBD)][BAr$^F_4$], [**3-NBD**][**BAr$^F_4$**], was prepared in an analogous manner to [**2-NBD**][**BAr$^F_4$**] (Scheme 4). This could be isolated as an orange/red crystalline

Scheme 4. Addition of H_2 to [3-NBD][BAr$^F_4$] in the Solid State

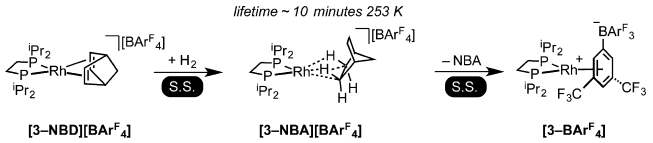

material. Interestingly the solid-state structure shows that the packing motif for the [BAr$^F_4$]$^-$ anions is not octahedral around the cation, but instead eight anions adopt a gyrobifastigium arrangement (formed from two face-sharing trigonal prisms, Supporting Information, Figure S1). There is no crystallographically imposed symmetry in this cation. Again, as for [**2-NBA**][**BAr$^F_4$**], weak C−H···F−C hydrogen bonding is apparent between the cation and the CF_3 groups. The ^{31}P{^{1}H} SSNMR of [**3-NBD**][**BAr$^F_4$**] shows an ABX pattern, consistent with crystallographically independent phosphorus environments. Addition of H_2 to [**3-NBD**][**BAr$^F_4$**] in a solid/gas reaction and following the temporal evolution of products by ^{31}P{^{1}H} SSNMR spectroscopy at 253 K revealed, after 11 min, an intermediate observed as an ABX spin system at chemical shifts and coupling constants similar to [**2-NBA**][**BAr$^F_4$**] [δ 113, J(RhP) = 193 Hz; δ 116, J(RhP) = 195 Hz]. This product is assigned to the σ-alkane complex [Rh(^{i}Pr$_2$PCH$_2$CH$_2$P^{i}Pr$_2$)(NBA)][BAr$^F_4$], [**3-NBA**][**BAr$^F_4$**]. This, however, is not the major species observed. Rather, a broad signal centered at δ 103 dominates which is assigned to an amorphous phase of the [BAr$^F_4$]$^-$-coordinated final product [**3-BAr$^F_4$**]. Warming to 298 K resulted in the disappearance of signals due to [**3-NBA**][**BAr$^F_4$**]. On gentle heating to 323 K amorphous [**3-BAr$^F_4$**] undergoes a phase change to give crystalline material, and corresponding sharp signals are observed [δ 102, J(RhP) = 203 Hz; δ 98, J(RhP) = 195 Hz] (Supporting Information, Figure S5). A similar phase change (at 298 K) was reported for [**1-BAr$^F_4$**].[59] Despite repeated attempts we could not obtain single crystals of [**3-NBA**][**BAr$^F_4$**] suitable for an X-ray diffraction study, due to it being short-lived. However, DFT calculations on the [**3-NBA**]$^+$ cation suggest its structure will be closely related to that of [**2-NBA**]$^+$ (Supporting Information, Table S2). Thus, despite being closely related to [**1-NBD**][**BAr$^F_4$**] and [**2-NBD**][**BAr$^F_4$**], hydrogenation in the solid state of [**3-NBD**][**BAr$^F_4$**] only fleetingly produces a complex with NMR data consistent with the σ-alkane complex [**3-NBA**][**BAr$^F_4$**].

Yellow/orange crystals suitable for a single-crystal X-ray diffraction study of zwitterion [**3-BAr$^F_4$**] were obtained by recrystallization of the material produced via the solid/gas synthesis, using a C_6F_6/pentane solvent system. The structure is unremarkable, and very similar to those described for [**1-BAr$^F_4$**][59] and [**2-BAr$^F_4$**] adopting what might be best described as an η^5-aryl binding motif in the solid state (Supporting Information, Figure S6).

2.4. [Rh(^{i}Pr$_2$PCH$_2$CH$_2$CH$_2$P^{i}Pr$_2$)]$^+$. Interested in keeping the P-alkyl groups the same, but varying the bite-angle[105] of the chelating phosphine, we prepared [Rh(^{i}Pr$_2$PCH$_2$CH$_2$CH$_2$P^{i}Pr$_2$)(NBD)][BAr$^F_4$], [**4-NBD**][**BAr$^F_4$**], for which orange crystals suitable for single-crystal X-ray diffraction could be grown from CH_2Cl_2/pentane solution. Although the extended solid-state structure shows the familiar octahedral arrangement of [BAr$^F_4$]$^-$ anions around each of the [Rh(^{i}Pr$_2$PCH$_2$CH$_2$CH$_2$P^{i}Pr$_2$)(NBD)]$^+$ cations, in this case there are two independent cations in the unit cell, one of which lies on a crystallographically imposed mirror plane. The structure could be accurately solved using a unit cell that contained 12 cations (space group $C2/c$), see Figure 9A, and leads to three crystallographically different phosphorus environments in the solid state. Other structural metrics are unremarkable, and there are also a number of weak C−H···F−C hydrogen bonds (2.4−2.8 Å) present, as for [**2-NBD**][**BAr$^F_4$**] and [**2-NBA**][**BAr$^F_4$**]. The ^{31}P{^{1}H} SSNMR of [**4-NBD**][**BAr$^F_4$**] shows at least two overlapping signals (Figure 8), one much broader than the other, at δ 21 and 19,

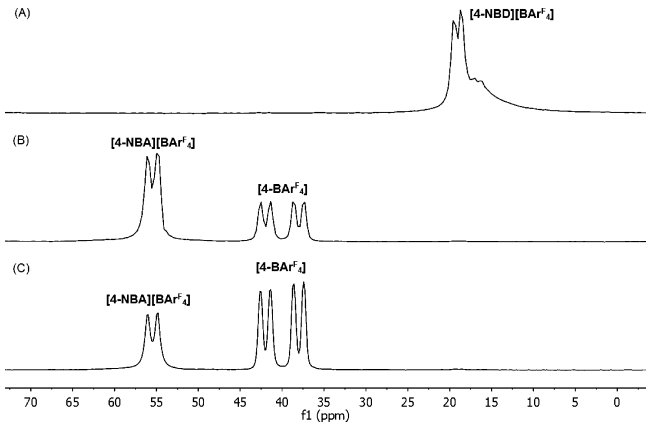

Figure 8. ^{31}P{^{1}H} SSNMR spectra of H_2 addition to powdered crystalline [**4-NBD**][**BAr$^F_4$**], 298 K: (A) [**4-NBD**][**BAr$^F_4$**], (B) after H_2 addition (4 atm, 9 min, then argon for 21 min), and (C) after 4.5 h.

respectively. This difference in line width between these two signals is marked, perhaps reflecting the symmetry attributes of the extended unit cell in [**4-NBD**][**BAr$^F_4$**].

Addition of H_2 to crystalline [**4-NBD**][**BAr$^F_4$**] in a solid/gas reaction resulted in a immediate change in color from orange to claret-red (Scheme 5). Following this process using ^{31}P{^{1}H} SSNMR spectroscopy at 298 K showed the formation of a complex with a spectral signature consistent with the formation of [**4-NBA**][**BAr$^F_4$**], as indicated by a broad signal at δ 56 [J(RhP) ≈ 191 Hz] which has doublet character. This complex is considerably more persistent than [**1-NBA**][**BAr$^F_4$**], taking

DOI: 10.1021/ja510437p
J. Am. Chem. Soc. 2015, 137, 820−833

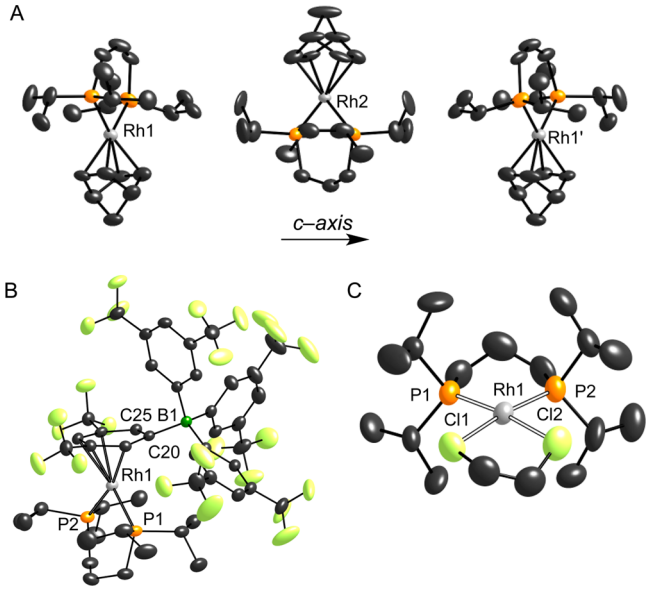

Figure 9. (A) View across the crystallographic *c*-axis for the cation [**4-NBD**]$^+$ (BAr^F_4 anions omitted) showing the modulated structure in which the asymmetric unit contains 1.5 cations. (B) Solid-state structure of [**4-BAr$^F_4$**]. Selected bond lengths (Å) and angles (deg): Rh1–P1, 2.2746(7); Rh1–P2, 2.2637(7); Rh1–C21, 2.334(2); Rh1–C22, 2.313(3); Rh1–C20, 2.552(2); Rh1–C25, 2.486(3); P1–Rh1–P2, 92.23(3). (C) Solid-state structure of [**4-DCE**] showing the major disorder component for the DCE ligand. Selected bond lengths (Å): Rh1–P1, 2.204(3); Rh1–P2, 2.209(3); Rh1–Cl1, 2.458(4); Rh1–Cl2, 2.434(4). Displacement ellipsoids are shown at the 50% probability levels.

Scheme 5. Addition of H_2 to [4-NBD][BAr$^F_4$] in the Solid State

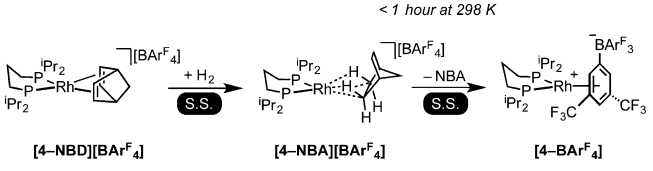

over 12 h to form orange-yellow [**4-BAr$^F_4$**] at 298 K, as identified by its independent synthesis (eq 2); however, it is

$$[\textbf{4-NBA}][\textbf{BAr}^{\textbf{F}}_4] \xrightarrow[\text{2. cool}]{\text{1. hexane, 313 K, 1 h}} [\textbf{4-BAr}^{\textbf{F}}_4] \qquad (2)$$

likely that crystal size influences the rate of this change, as commented upon for [**1-NBA**][**BAr$^F_4$**].[59] At 233 K complex [**4-NBA**][**BAr$^F_4$**] appears to be stable by $^{31}P\{^1H\}$ SSNMR spectrometry, with the transformation to [**4-BAr$^F_4$**] halted. There also appears to be no loss of single-crystallinity on addition of H_2 in the solid state. However, despite repeated attempts, crystalline material that produced a reliable crystallographic solution for the structure of [**4-NBA**][**BAr$^F_4$**] was not forthcoming,[106] although a partial structure showed the approximate heavy-atom positions of the cation.

The structure of the final product [**4-BAr$^F_4$**] (Figure 9B) reveals that the coordinated [BAr^F_4]$^-$ anion has slipped with the aryl ring binding with the metal center in an η^4-motif, with two longer Rh–C distances: Rh–C20, 2.552(2) Å and Rh–C(25), 2.486(3) Å. The greater slippage compared to [**3-BAr$^F_4$**], is also captured by the DFT calculations and so presumably reflects the steric and electronic demands of the wider bite angle ligand: [**4-BAr$^F_4$**], P–Rh–P, 92.23(3)°; [**3-BAr$^F_4$**], 84.14(3)°. It is also reflected in the lack of stability of [**4-BAr$^F_4$**] in CD_2Cl_2 solution, with immediate decomposition occurring at 298 K to form unidentified species; solution ^{31}P and ^{19}F NMR data were therefore collected in H_{12}-pentane and are consistent with the solid-state structure. A $^{13}C\{^1H\}$ SSNMR spectrum of [**4-BAr$^F_4$**] shows characteristic signals between δ 90 and 98 assignable to the bound aryl group of the anion.

Vacuum transfer of CD_2Cl_2 onto claret-red [**4-NBA**][**BAr$^F_4$**] immediately after addition of hydrogen to [**4-NBD**][**BAr$^F_4$**] and placing in a pre-cooled NMR spectrometer at 188 K resulted in a bright-red solution that showed free NBA by ^1H NMR spectroscopy. A single environment was observed in the $^{31}P\{^1H\}$ NMR spectrum at that temperature, with a large coupling constant to ^{103}Rh [δ 51.0, J(RhP) = 199 Hz] and no evidence for [**4-BAr$^F_4$**]. We therefore assign a structure either to a solvent complex (CD_2Cl_2)[107,108] or a complex stabilized by agostic Rh···H–C interactions;[109] although for the latter there was no evidence of high field signals in the ^1H NMR spectrum that might be attributed to such interactions, these are likely fluxional. Warming this solution to room temperature resulted in decomposition. However, repeating this experiment using 1,2-dichloroethane (DCE) solvent afforded complex [**4-DCE**][**BAr$^F_4$**] (alongside free NBA), which was assigned spectroscopically and by single-crystal X-ray diffraction as [Rh(^{i}Pr$_2$PCH$_2$CH$_2$CH$_2$P^{i}Pr$_2$)(κ^2-Cl$_2$C$_2$H$_4$)][BAr^F_4], [**4-DCE**][**BAr$^F_4$**], eq 3. Figure 9C shows the solid-state structure,

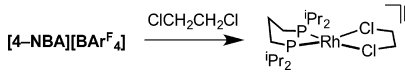

(Eq. 3)

which demonstrates chelation of one DCE to the Rh(I) center through two Rh–Cl interactions. Isolated DCE complexes are surprisingly rare,[70,110,111] even though this is a common solvent used in synthesis and catalysis. In DCE solution the room temperature $^{31}P\{^1H\}$ NMR spectrum shows a single environment at δ 50.2 [J(RhP) 190 Hz] that is very similar to that observed for the product formed from solvation of [**4-NBA**][**BAr$^F_4$**] at low temperature in CD_2Cl_2, perhaps suggesting a solvent adduct is also formed under these conditions. Solvent (CDF_2Cl) adducts have also been suggested for complex **C** (on warming and loss of alkane)[49,51] and when [**1-NBA**][**BAr$^F_4$**] is dissolved in this solvent.[59]

2.5. [Rh{(^{i}PrO)$_2$PCH$_2$CH$_2$P(O^{i}Pr)$_2$}]$^+$. As well as changing the steric environment of the phosphine, it was of interest to vary the electronics of the chelating ligand, in the anticipation that this would lead to a more persistent alkane complex. Changing to a more electron-withdrawing phosphite was attractive as calculations on [M(pincer)(methane)]$^+$ (M = Rh, Ir) systems have indicated that electron-withdrawing groups enhance the binding strength of the alkane.[50] The isopropoxide ligand (^{i}PrO)$_2$PCH$_2$CH$_2$P(O^{i}Pr)$_2$ was chosen,[112] as this maintains steric parameters similar to those of the isobutyl ligand in **1** but is likely to have significantly different electronic properties associated with the π-acidic phosphites.

Addition of H_2 to crystalline orange/red [Rh{(^{i}PrO)$_2$PCH$_2$CH$_2$P(O^{i}Pr)$_2$}(NBD)][BAr^F_4], [**5-NBA**][**BAr$^F_4$**],[113] led to the immediate formation of pale yellow [**5-BAr$^F_4$**] at 253 K (Scheme 6). No alkane intermediate was observed by *in situ* $^{31}P\{^1H\}$ SSNMR spectroscopy and [**5-BAr$^F_4$**] is formed as an amorphous solid (Figure S8). Recrystallization from pentane yields single crystals suitable

DOI: 10.1021/ja510437p
J. Am. Chem. Soc. 2015, 137, 820–833

Scheme 6

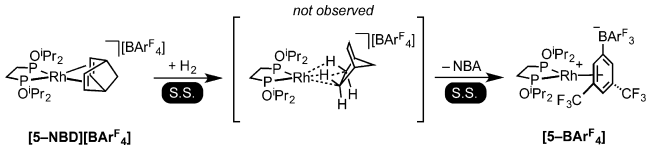

for an X-ray diffraction study (Supporting Information, Table S1), which shows a $[BAr^F_4]^-$ anion coordinated to the metal fragment, with structural metrics very similar to those reported previously. Thus, in this case the more electron-withdrawing phosphite ligands do not stabilize the intermediate alkane complex.

3. COMPUTATIONAL STUDIES

DFT calculations have been employed to analyze the geometry and bonding in the molecular σ-alkane $[\mathbf{2\text{-}NBA}]^+$ cation within $[\mathbf{2\text{-}NBA}][\mathbf{BAr^F_4}]$. Geometries were optimized using the BP86 functional, our previous study having shown this method provides good comparison with experimental data for the $[\mathbf{1\text{-}NBA}]^+$ cation in $[\mathbf{1\text{-}NBA}][\mathbf{BAr^F_4}]$ and that it also performs well against a range of other functionals.[59,114] We have also considered the $[\mathbf{Y\text{-}NBA}]^+$ cations in $[\mathbf{Y\text{-}NBA}][\mathbf{BAr^F_4}]$ (Y = 3–5) and the molecular zwitterions in $[\mathbf{Y\text{-}BAr^F_4}]$ (Y = 1–5) to shed light on the factors determining the relative stabilities of the σ-alkane complexes. Initial geometries for optimization were derived from the relevant crystallographically determined structures or, when not available (as is the case for $[\mathbf{Y\text{-}NBA}]^+$, Y = 3–5), were adapted from the NBD precursor. The above discussion of the crystallographic structures highlighted the good agreement between experiment and computation for a range of key structural parameters and a full comparison is provided in the Supporting Information (Figure S9 and Tables S2 and S3).

3.1. Electronic Structure of $[\mathbf{2\text{-}NBA}]^+$. The presence of two C–H → Rh σ-interactions in $[\mathbf{2\text{-}NBA}]^+$ is confirmed by an analysis of the topology of the total electron density using the quantum theory of atoms-in-molecules (QTAIM) approach (see Figure 10). Curved bond paths between Rh and both H11 and H21 are seen, and these, in combination with the properties of the associated bond critical points (BCPs) are consistent with the presence of two equivalent σ-interactions (electron density, $\rho(r)$ = 0.060 au; Laplacian, $\nabla^2\rho(r)$ = 0.208, and total energy density, $H(r)$ = −0.013 au; data are for the Rh···H11 BCP).[115–119] As already noted above, this σ-interaction causes elongation and weakening of the C1–H11 and C2–H21 bonds and this is also reflected in the properties of the associated BCPs. Thus, compared to the spectator C1–H12, the C1–H11 bond shows reduced values for $\rho(r)$ (0.231 cf. 0.274), $\nabla^2\rho(r)$ (−0.610 cf. −0.929) and H(r) (−0.198 cf. −0.274). Coordination to the Rh center also causes a red-shift in the computed C–H stretching frequencies (C1–H11/C2–H21: ν_{C-H}(sym) = 2430 cm^{-1}, ν_{C-H}(asym) = 2455 cm^{-1} cf. C1–H12/C2–H22: ν_{C-H}(sym) = 3046 cm^{-1}, ν_{C-H}(asym) = 3039 cm^{-1}; unscaled values). The presence of a ring critical point (RCP) approximately midway between Rh and the center of the C1–C2 bond is consistent with the chelating binding mode of the bidentate NBA ligand; no evidence for any C–C → Rh agostic interaction is seen.[120]

Key molecular orbitals of the $[\mathbf{2\text{-}NBA}]^+$ cation are shown in Figure 11. The high lying occupied orbitals are consistent with a Rh(I) complex exhibiting a square-planar coordination

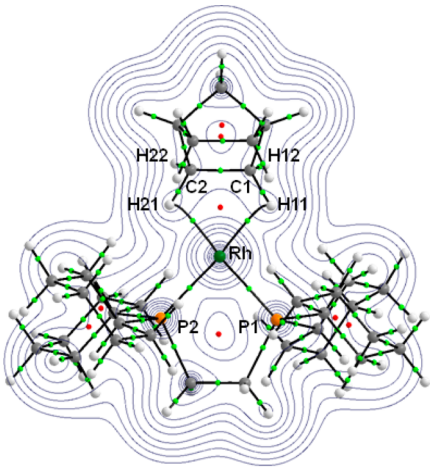

BCP	ρ(r)	∇²ρ(r)	H(r)
Rh···H11	0.060	0.208	−0.013
C1–H11	0.231	−0.610	−0.198
C1–H12	0.274	−0.929	−0.274

Figure 10. Contour plots of the electron density of the $[\mathbf{2\text{-}NBA}]^+$ cation presented in the {RhH11H21} plane, with projected stationary points and bond paths. Bond critical points (BCP) are shown in green and ring critical points (RCP) in red. Calculated QTAIM parameters (au) for selected BCPs are shown ($\rho(r)$ = electron density, $\nabla^2\rho(r)$ = Laplacian of electron density; $H(r)$ = local energy density). For full summary of parameters see Table S5.

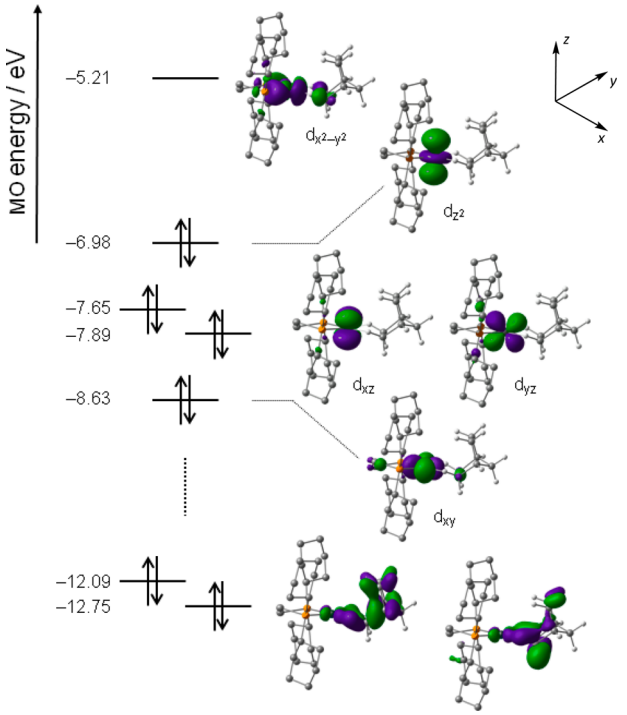

Figure 11. Key computed molecular orbitals of the $[\mathbf{2\text{-}NBA}]^+$ cation. Orbitals energies are in eV, and boundary surfaces are drawn with a cutoff of 0.05 e Å^{-3}.

geometry. Thus, four high-lying occupied d-orbitals are apparent, with the HOMO (E = −6.98 eV) being dominated by Rh(d_{z^2}) character. Below this lie two essentially non-bonding d_{xz} and d_{yz} orbitals, while the d_{xy} orbital (E = −8.63 eV) is stabilized via π-back-donation interactions with the σ* ABMOs of the C1–H11 and C2–H21 bonds. The LUMO is

DOI: 10.1021/ja510437p
J. Am. Chem. Soc. 2015, 137, 820–833

predominantly $d_{x^2-y^2}$ in character and is M−L σ-antibonding with both the phosphorus centers and the C1−H11 and C2−H21 σ-BMOs. A significant HOMO−LUMO gap of 1.77 eV is computed. Evidence for Rh−alkane σ-bonding interactions is seen in two low-energy σ-BMOs (E = −12.09, −12.75 eV). A fragment analysis suggests that a large number of NBA orbitals contribute to these, making further interpretation on the basis of these delocalized MOs alone problematic.

In order to place the bonding interactions between the NBA ligand and the cationic $\{Rh(L_2)\}^+$ fragment on a more quantitative footing NBO analyses were performed on [**2-NBA**]$^+$. Important donor−acceptor pairs within [**2-NBA**]$^+$ are

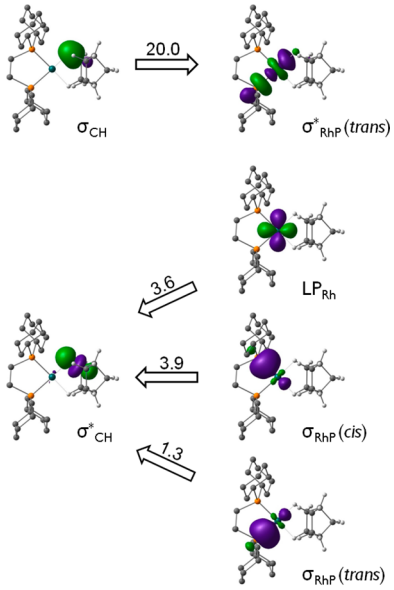

Figure 12. Important natural bond orbitals (NBOs) involved in donor/acceptor interactions in [**2-NBA**]$^+$ (top view) along with their second-order perturbation energies (in kcal/mol).

shown in Figure 12 along with the associated interaction energies, $\Delta E^{(2)}$, quantified using second order perturbation theory. NBA coordination arises via σ-donation from the σ_{CH} orbital into the vacant *trans*-σ^*_{RhP} orbital ($\Delta E^{(2)}$ = 20.0 kcal/mol). This is reinforced by back-donation from a Rh lone pair (corresponding to the d_{xy} orbital) into the unoccupied σ^*_{CH} orbital ($\Delta E^{(2)}$ = 3.6 kcal/mol), further enhanced by donation from both the *cis*- and *trans*-σ_{RhP} orbitals ($\Delta E^{(2)}$ = 3.9 and 1.3 kcal/mol, respectively, giving a total back-donation of 8.7 kcal/mol). σ_{CH} → Rh donation is therefore the major component of the Rh−alkane interaction, this being more than twice that of σ^*_{CH} ← Rh back-donation. Overall, these σ-interactions in [**2-NBA**]$^+$ are relatively weak, as shown by comparing with the π-interactions of the C═C double bond of the NBD ligand in [**2-NBD**]$^+$ (π_{CC} → *trans*-σ^*_{RhP} = 56.3 kcal/mol; LP_{Rh} (π) → π^*_{CC} = 36.1 kcal/mol). We have also assessed the possibility of a C1−C2···[Rh] σ-interaction in [**2-NBA**]$^+$, but the small stabilization energy ($\Delta E^{(2)} \approx$ 0.5 kcal/mol) arising from two separate σ_{CC} → σ^*_{RhP} donations indicates this interaction is negligible.

3.2. Comparison of Cationic σ-Alkane Complexes [Y-NBA]$^+$ (Y = 1−5). The above computational analyses were repeated for the related cations [**Y-NBA**]$^+$ (Y = 3−5) which, combined with data from our previous study on [**1-NBA**]$^+$, allowed for comparison across this series of σ-alkane complexes. These five cations, as their $[BAr^F_4]^-$ salts, show widely different stabilities in the solid state, from being unobservable (Y = 5) to being observable for minutes (Y = 3), hours (Y = 1, 4) or even months (Y = 2). The computed structures of the [**Y-NBA**]$^+$ cations, however, show relatively little variation in the key computed distances across the series (Rh···H11, 1.903−1.932 Å; C1−H11, 1.153−1.158 Å). This is also reflected in a narrow range computed for the BCP parameters and $\Delta E^{(2)}$ values derived from the QTAIM and NBO studies, respectively, as well as the computed C−H stretching frequencies associated with the Rh···C−H bonds (see Supporting Information, Tables S4−S6). No correlation is therefore evident between the geometric or electronic properties of the free cations and their relative stabilities in the solid state. Experimentally the [**Y-NBA**][**BAr$^F_4$**] species transform into the [**Y-BAr$^F_4$**] species via displacement of the alkane by the $[BAr^F_4]^-$ anion. To assess how the free energy of this exchange process (ΔG_3, Table 1) varies across the series of [**Y-NBA**]$^+$ cations we computed the free energy changes for (i) NBA dissociation (ΔG_1) and (ii) $[BAr^F_4]^-$ addition (ΔG_2) to form the molecular zwitterions seen in the [**Y-BAr$^F_4$**] structures.

Table 1. Computed Free Energies (BP86-D3 Level, kcal/mol) for NBA/$[BAr^F_4]^-$ Substitution in the Isolated [Y-NBA]$^+$ Cations To Give the [Y-BAr$^F_4$] Molecular Zwitterions (Y = 1−5)

[**Y-NBA**]$^+$ $\xrightarrow{\text{(i) − NBA}}$ [**Y-NBA**]$^+$ $\xrightarrow{\text{(ii) + } [BAr^F_4]^-}$ [**Y-BAr$^F_4$**]$^+$

	ΔG_1	ΔG_2	ΔG_3
Y = 1, $^iBu_2P(CH_2)_2P^iBu_2$	13.5	−94.4	−80.9
Y = 2, $Cy_2P(CH_2)_2PCy_2$	18.5	−98.1	−79.6
Y = 3, $^iPr_2P(CH_2)_2P^iPr_2$	18.4	−99.1	−80.7
Y = 4, $^iPr_2P(CH_2)_3P^iPr_2$	16.1	−93.0	−76.9
Y = 5, $(^iPrO)_2P(CH_2)_2P(O^iPr)_2$	13.8	−104.5	−90.7

This approach yields alkane binding energies between 13.5 and 18.5 kcal/mol, with the subsequent $[BAr^F_4]^-$ binding energies all being in excess of 90 kcal/mol. The large values for the latter reflect the favorable electrostatics associated with formation of the [**Y-BAr$^F_4$**] molecular zwitterions, which is maximized with electron-withdrawing O^{i}Pr substituents (Y = 5). The free energies of NBA/$[BAr^F_4]^-$ exchange for this molecular model are thus all highly exergonic. Moreover, very similar values are found for Y = 2 (−79.6 kcal/mol) and Y = 3 (−80.7 kcal/mol) despite the very different stabilities seen experimentally for the [**Y-NBA**][**BAr$^F_4$**] alkane complexes in the solid state. These results indicate that variations in Rh−NBA bonding alone cannot account for the different stabilities of these alkane complexes and that the detailed crystal environment is essential in conferring the necessary kinetic (and possibly in the case of [**2-NBA**][**BAr$^F_4$**] thermodynamic) stability on the σ-alkane complexes in the solid state.

4. CONCLUSIONS

Through manipulation of the identity of the supporting bidentate phosphine ligand (i.e., $Cy_2PCH_2CH_2PCy_2$) we have been able to synthesize a remarkably stable example of a σ-alkane complex [**2-NBA**][**BAr$^F_4$**] by a solid−gas crystal to crystal synthetic route. The stability of this complex has allowed for both accurate determination of the solid-state structure, including hydrogen positions for the Rh···H−C σ interactions, as well as solid-state NMR spectroscopic data to be collected in

DOI: 10.1021/ja510437p
J. Am. Chem. Soc. 2015, 137, 820−833

which these interactions can also be observed in the ^{1}H NMR spectrum. Complementary DFT calculations aid the NMR assignments as well as dissecting the bonding between the $\{Rh(L_2)\}^+$ fragment and NBA, in which $\sigma_{CH} \rightarrow$ Rh donation is the major component of the interaction, being more than twice that of $\sigma^*_{CH} \leftarrow$ Rh back-donation. An alkane binding energy of 18.5 kcal/mol is calculated for the [**2-NBA**]$^+$ cation. Although [**2-NBA**][**BAr$^F_4$**] loses alkane (NBA) when dissolved in solution ($CDCl_2F$) to form a zwitterionic complex, [**2-BAr$^F_4$**], we believe this to be the most completely characterized σ-alkane complex yet reported. The enhanced stability of [**2-NBA**][**BAr$^F_4$**] with respect to [**2-BAr$^F_4$**] in the solid state contrasts with that of other closely related bidentate alkyl phosphine and phosphite ligands in which subtle changes to both the P-substituents (^{i}Bu, ^{i}Pr, O^{i}Pr) or chelate backbone (^{i}Pr$_2$PCH$_2$CH$_2$CH$_2$P^{i}Pr$_2$) result in either relatively short-lived σ-alkane complexes (by ^{31}P SSNMR spectroscopy) or the immediate formation of the [BAr$^F_4$]$^-$-coordinated final product in the solid state. However, DFT calculations on the free σ-alkane cations show that there is little difference in the strength of alkane binding in any of these NBA complexes, and that the displacement of NBA by a [BAr$^F_4$]$^-$ anion is highly exergonic with very similar values being calculated for all cases (−80 to −90 kcal/mol). The remarkable stability of [**2-NBA**][**BAr$^F_4$**] may therefore be due to kinetic factors, e.g., re-organization energy associated with loss of the alkane and disruption of the local anion environment in the solid state. In this regard we note that cyclohexyl groups are likely the most rigid of the substituents studied here, and this might influence the barrier to reorganization. However, we cannot discount that thermodynamic factors in the solid state, that will not be treated by our current DFT calculations, might well cause complex [**2-NBA**][**BAr$^F_4$**] to be particularly stable with regard to [**2-BAr$^F_4$**]. In this regard the weak C−H···F−C hydrogen bonding observed in all the structures might be important. An assessment by computational means of the role of the extended lattice structure on σ-alkane complex stability is thus the subject of ongoing work. Moreover, the mechanism by which the H_2 adds to the alkene fragment and re-organization occurs to yield the final NBA product will be reported upon in a future contribution. Finally, as part of this study, we have synthesized and characterized in the solid state a large number of [BAr$^F_4$]$^-$-coordinated zwitterions, adding to the relatively small number of previously reported examples of this coordination motif of this weakly coordinating anion.

Overall, we have presented evidence for a number of new σ-alkane complexes of the general formula [Rh(chelating-phosphine)(NBA)][BAr$^F_4$]. These add to the still relatively small, but growing,[14] number examples of this fascinating and important set of coordination complexes. It will be interesting to explore if the NBA−alkane motif we have developed here and previously[59] is unique in allowing for the synthesis and characterization of such species in the solid state, or if other metal/supporting ligand/alkane combinations also offer the same degree of relative stability.

■ ASSOCIATED CONTENT

Supporting Information

Experimental and characterization details, including NMR spectroscopic data, X-ray crystallographic data, and computational details. This material is available free of charge via the Internet at http://pubs.acs.org. Crystallographic data have been deposited with the Cambridge Crystallographic Data Center (CCDC) and can be obtained via www.ccdc.cam.ac.uk/data_request/cif, 1022725-1022727; 1022729-1022733.

■ AUTHOR INFORMATION

Corresponding Authors

andrew.weller@chem.ox.ac.uk
s.a.macgregor@hw.ac.uk

Notes

The authors declare no competing financial interest.

■ ACKNOWLEDGMENTS

We thank the EPSRC EP/K035908/1 and EP/K035681/1 for funding, and the EPSRC National Solid-State NMR Service (Durham), especially Dr. David Applerley, for the collection of the solid-state ^{31}P{^{1}H} NMR spectra of complexes **3**, **4**, and **5**.

■ REFERENCES

(1) Hammond, C.; Conrad, S.; Hermans, I. *ChemSusChem* **2012**, *5*, 1668−1686.
(2) Crabtree, R. H. *Chem. Rev.* **2010**, *110*, 575.
(3) Labinger, J. A.; Bercaw, J. E. *Nature* **2002**, *417*, 507−514.
(4) Shilov, A. E.; Shul'pin, G. B. *Activation and Catalytic Reactions of Saturated Hydrocarbons in the Presence of Metal Complexes*; Kluwer: Dordrecht, 2000.
(5) *Activation and Functionalization of C−H Bonds*; Goldberg, K. I., Goldman, A. S., Eds.; American Chemical Society: Washington, DC, 2004; Vol. *85*.
(6) Bergman, R. G. *Nature* **2007**, *446*, 391−393.
(7) *Alkane C−H Activation by Single-Site Metal Catalysis*; Pérez, P. J., Ed.; Springer: Dordrecht, 2012; Vol. *38*.
(8) Arndtsen, B. A.; Bergman, R. G.; Mobley, T. A.; Peterson, T. H. *Acc. Chem. Res.* **1995**, *28*, 154−162.
(9) Kubas, G. J. *Metal Dihydrogen and σ-Bond Complexes*; Kluwer: New York, 2001.
(10) Perutz, R. N.; Sabo-Etienne, S. *Angew. Chem., Int. Ed.* **2007**, *46*, 2578−2592.
(11) Hall, C.; Perutz, R. N. *Chem. Rev.* **1996**, *96*, 3125−3146.
(12) Cobar, E. A.; Khaliullin, R. Z.; Bergman, R. G.; Head-Gordon, M. *Proc. Natl. Acad. Sci. U.S.A.* **2007**, *104*, 6963−6968.
(13) Cowan, A. J.; Portius, P.; Kawanami, H. K.; Jina, O. S.; Grills, D. C.; Sun, X. Z.; McMaster, J.; George, M. W. *Proc. Natl. Acad. Sci. U.S.A.* **2007**, *104*, 6933−6938.
(14) Young, R. D. *Chem. Eur.—J.* **2014**, *20*, 12704−12718.
(15) Shilov, A. E.; Shul'pin, G. B. *Chem. Rev.* **1997**, *97*, 2879−2932.
(16) Periana, R. A.; Taube, D. J.; Gamble, S.; Taube, H.; Satoh, T.; Fujii, H. *Science* **1998**, *280*, 560−564.
(17) Periana, R. A.; Mironov, O.; Taube, D.; Bhalla, G.; Jones, C. J. *Science* **2003**, *301*, 814−818.
(18) Lersch, M.; Tilset, M. *Chem. Rev.* **2005**, *105*, 2471−2526.
(19) Stahl, S. S.; Labinger, J. A.; Bercaw, J. E. *Angew. Chem., Int. Ed.* **1998**, *37*, 2180−2192.
(20) Mironov, O. A.; Bischof, S. M.; Konnick, M. M.; Hashiguchi, B. G.; Ziatdinov, V. R.; Goddard, W. A.; Ahlquist, M.; Periana, R. A. *J. Am. Chem. Soc.* **2013**, *135*, 14644−14658.
(21) Chen, G. S.; Labinger, J. A.; Bercaw, J. E. *Proc. Natl. Acad. Sci. U.S.A.* **2007**, *104*, 6915−6920.
(22) Munz, D.; Meyer, D.; Strassner, T. *Organometallics* **2013**, *32*, 3469−3480.
(23) Jones, W. D. *Inorg. Chem.* **2005**, *44*, 4475−4484.
(24) Jones, W. D. *Acc. Chem. Res.* **2003**, *36*, 140−146.
(25) Bercaw, J. E.; Chen, G. S.; Labinger, J. A.; Lin, B.-L. *J. Am. Chem. Soc.* **2008**, *130*, 17654−17655.
(26) Fekl, U.; Goldberg, K. I. *J. Am. Chem. Soc.* **2002**, *124*, 6804−6805.
(27) Gérald, H.; Eisenstein, O.; Lee, D.-H.; Chen, J.; Crabtree, R. H. *New J. Chem.* **2001**, *25*, 1121−1131.

DOI: 10.1021/ja510437p
J. Am. Chem. Soc. 2015, 137, 820−833

(28) Choi, J.; MacArthur, A. H. R.; Brookhart, M.; Goldman, A. S. *Chem. Rev.* **2011**, *111*, 1761−1779.
(29) Haibach, M. C.; Kundu, S.; Brookhart, M.; Goldman, A. S. *Acc. Chem. Res.* **2012**, *45*, 947−958.
(30) Mkhalid, I. A. I.; Barnard, J. H.; Marder, T. B.; Murphy, J. M.; Hartwig, J. F. *Chem. Rev.* **2010**, *110*, 890−931.
(31) Hashiguchi, B. G.; Konnick, M. M.; Bischof, S. M.; Gustafson, S. J.; Devarajan, D.; Gunsalus, N.; Ess, D. H.; Periana, R. A. *Science* **2014**, *343*, 1232−1237.
(32) Bloch, E. D.; Queen, W. L.; Krishna, R.; Zadrozny, J. M.; Brown, C. M.; Long, J. R. *Science* **2012**, *335*, 1606−1610.
(33) Geier, S. J.; Mason, J. A.; Bloch, E. D.; Queen, W. L.; Hudson, M. R.; Brown, C. M.; Long, J. R. *Chem. Sci.* **2013**, *4*, 2054−2061.
(34) Herm, Z. R.; Bloch, E. D.; Long, J. R. *Chem. Mater.* **2013**, *26*, 323−338.
(35) Poliakoff, M.; Turner, J. J. *J. Chem. Soc., Dalton Trans.* **1974**, 2276−2285.
(36) Perutz, R. N.; Turner, J. J. *J. Am. Chem. Soc.* **1975**, *97*, 4791−4800.
(37) McNamara, B. K.; Yeston, J. S.; Bergman, R. G.; Moore, C. B. *J. Am. Chem. Soc.* **1999**, *121*, 6437−6443.
(38) Blake, A. J.; George, M. W.; Hall, M. B.; McMaster, J.; Portius, P.; Sun, X. Z.; Towrie, M.; Webster, C. E.; Wilson, C.; Zaric, S. D. *Organometallics* **2008**, *27*, 189−201.
(39) Cowan, A. J.; George, M. W. *Coord. Chem. Rev.* **2008**, *252*, 2504−2511.
(40) Pitts, A. L.; Wriglesworth, A.; Sun, X. Z.; Calladine, J. A.; Zarić, S. D.; George, M. W.; Hall, M. B. *J. Am. Chem. Soc.* **2014**, *136*, 8614−8625.
(41) Geftakis, S.; Ball, G. E. *J. Am. Chem. Soc.* **1998**, *120*, 9953−9954.
(42) Lawes, D. J.; Geftakis, S.; Ball, G. E. *J. Am. Chem. Soc.* **2005**, *127*, 4134−4135.
(43) Lawes, D. J.; Darwish, T. A.; Clark, T.; Harper, J. B.; Ball, G. E. *Angew. Chem., Int. Ed.* **2006**, *45*, 4486−4490.
(44) Calladine, J. A.; Duckett, S. B.; George, M. W.; Matthews, S. L.; Perutz, R. N.; Torres, O.; Vuong, K. Q. *J. Am. Chem. Soc.* **2011**, *133*, 2303−2310.
(45) Duckett, S. B.; George, M. W.; Jina, O. S.; Matthews, S. L.; Perutz, R. N.; Sun, X.-Z.; Vuong, K. Q. *Chem. Commun.* **2009**, 1401−1403.
(46) Young, R. D.; Hill, A. F.; Hillier, W.; Ball, G. E. *J. Am. Chem. Soc.* **2011**, *133*, 13806−13809.
(47) Young, R. D.; Lawes, D. J.; Hill, A. F.; Ball, G. E. *J. Am. Chem. Soc.* **2012**, *134*, 8294−8297.
(48) Calladine, J. A.; Torres, O.; Anstey, M.; Ball, G. E.; Bergman, R. G.; Curley, J.; Duckett, S. B.; George, M. W.; Gilson, A. I.; Lawes, D. J.; Perutz, R. N.; Sun, X.-Z.; Vollhardt, K. P. C. *Chem. Sci.* **2010**, *1*, 622−630.
(49) Bernskoetter, W. H.; Schauer, C. K.; Goldberg, K. I.; Brookhart, M. *Science* **2009**, *326*, 553−556.
(50) Walter, M. D.; White, P. S.; Schauer, C. K.; Brookhart, M. *New J. Chem.* **2011**, *35*, 2884−2893.
(51) Walter, M. D.; White, P. S.; Schauer, C. K.; Brookhart, M. *J. Am. Chem. Soc.* **2013**, *135*, 15933−15947.
(52) Evans, D. R.; Drovetskaya, T.; Bau, R.; Reed, C. A.; Boyd, P. D. W. *J. Am. Chem. Soc.* **1997**, *119*, 3633−3634.
(53) Castro-Rodriguez, I.; Nakai, H.; Gantzel, P.; Zakharov, L. N.; Rheingold, A. L.; Meyer, K. *J. Am. Chem. Soc.* **2003**, *125*, 15734−15735.
(54) Andreychuk, N. R.; Emslie, D. J. H. *Angew. Chem., Int. Ed.* **2013**, *125*, 1740−1743.
(55) Coville, N. J.; Cheng, L. *J. Organomet. Chem.* **1998**, *571*, 149−169.
(56) Albrecht, M.; Lutz, M.; Spek, A. L.; van Koten, G. *Nature* **2000**, *406*, 970−974.
(57) van der Boom, M. E. *Angew. Chem., Int. Ed.* **2011**, *50*, 11846−11848.
(58) Zenkina, O. V.; Keske, E. C.; Wang, R.; Crudden, C. M. *Angew. Chem., Int. Ed.* **2011**, *50*, 8100−8104.
(59) Pike, S. D.; Thompson, A. L.; Algarra, A. G.; Apperley, D. C.; Macgregor, S. A.; Weller, A. S. *Science* **2012**, *337*, 1648−1651.
(60) Vitórica-Yrezábal, I. J.; Mínguez Espallargas, G.; Soleimannejad, J.; Florence, A. J.; Fletcher, A. J.; Brammer, L. *Chem. Sci.* **2013**, *4*, 696−708.
(61) Xu, N.; Goodrich, L. E.; Lehnert, N.; Powell, D. R.; Richter-Addo, G. B. *Angew. Chem., Int. Ed.* **2013**, *52*, 3896−3900.
(62) Pike, S. D.; Weller, A. S. *Phil. Trans. R. Soc. A* **2014**, in press.
(63) Schrock, R. R.; Osborn, J. A. *J. Am. Chem. Soc.* **1976**, *98*, 2134−2143.
(64) Schrock, R. R.; Osborn, J. A. *J. Am. Chem. Soc.* **1976**, *98*, 2143−2147.
(65) Schrock, R. R.; Osborn, J. A. *J. Am. Chem. Soc.* **1976**, *98*, 4450−4455.
(66) Nguyen, B.; Brown, J. M. *Adv. Synth. Catal.* **2009**, *351*, 1333−1343.
(67) Hartwig, J. F. *OrganoTransition Metal Chemistry*; University Science Books: Sausalito, CA, 2010.
(68) Chaplin, A. B.; Weller, A. S. *Eur. J. Inorg. Chem.* **2010**, *2010*, 5124−5128.
(69) Pike, S. D.; Weller, A. S. *Dalton Trans.* **2013**, *42*, 12832−12834.
(70) Krossing, I. *Chem.—Eur. J.* **2001**, *7*, 490−502.
(71) In the previously reported (ref 59) 101 MHz $^{13}C\{^{1}H\}$ 10 kHz spin rate SSNMR spectrum of [**1-NBD**][$\mathbf{BAr^{F}_{4}}$], two broad signals at δ 68 and 65 were erroneously reported as being due to the phosphine ethylene bridge. Re-examination of this spectrum reveals one of these (δ 65) to be a spinning side-band associated with a broad aryl peak at δ 164, and the other (δ 68) is assigned to the bridgehead carbon of the NBD ligand.
(72) Apperley, D. C.; Harris, R. K.; Hodgkinson, P. *Solid-State NMR: Basic Principles & Practice*; Momentum Press: New York, 2012.
(73) Douglas, T. M.; Molinos, E.; Brayshaw, S. K.; Weller, A. S. *Organometallics* **2007**, *26*, 463−465.
(74) Lim, S. H.; Olmstead, M. M.; Balch, A. L. *Chem. Sci.* **2013**, *4*, 311−318.
(75) Alvarez, S. *Dalton Trans.* **2013**, *42*, 8617−8636.
(76) Yared, Y.; Miles, S.; Bau, R.; Reed, C. *J. Am. Chem. Soc.* **1977**, *99*, 7076−7078.
(77) Urtel, H.; Meier, C.; Eisenträger, F.; Rominger, F.; Joschek, J. P.; Hofmann, P. *Angew. Chem., Int. Ed.* **2001**, *40*, 781−784.
(78) Chaplin, A. B.; Poblador-Bahamonde, A. I.; Sparkes, H. A.; Howard, J. A. K.; Macgregor, S. A.; Weller, A. S. *Chem. Commun.* **2009**, 244−246.
(79) Chaplin, A. B.; Weller, A. S. *Organometallics* **2010**, *29*, 2332−2342.
(80) Chaplin, A. B. *Organometallics* **2014**, *33*, 3069−3077.
(81) Brayshaw, S. K.; Green, J. C.; Kociok-Köhn, G.; Sceats, E. L.; Weller, A. S. *Angew. Chem., Int. Ed.* **2006**, *45*, 452−456.
(82) Etienne, M.; Weller, A. S. *Chem. Soc. Rev.* **2014**, *43*, 242−259.
(83) Chaplin, A. B.; Weller, A. S. *J. Organomet. Chem.* **2013**, *730*, 90−94.
(84) Cordero, B.; Gómez, V.; Platero-Prats, A. E.; Revés, M.; Echeverría, J.; Cremades, E.; Barragán, F.; Alvarez, S. *Dalton Trans.* **2008**, 2832−2838.
(85) Delpech, F.; Sabo-Etienne, S.; Daran, J.-C.; Chaudret, B.; Hussein, K.; Marsden, C. J.; Barthelat, J.-C. *J. Am. Chem. Soc.* **1999**, *121*, 6668−6682.
(86) Grellier, M.; Mason, S. A.; Albinati, A.; Capelli, S. C.; Rizzato, S.; Bijani, C.; Coppel, Y.; Sabo-Etienne, S. *Inorg. Chem.* **2013**, *52*, 7329−7337.
(87) Cassen, A.; Gloaguen, Y.; Vendier, L.; Duhayon, C.; Poblador-Bahamonde, A. I.; Raynaud, C.; Clot, E.; Alcaraz, G.; Sabo-Etienne, S. *Angew. Chem., Int. Ed.* **2014**, *53*, 7569−7573.
(88) Johnson, H. C.; McMullin, C. L.; Pike, S. D.; Macgregor, S. A.; Weller, A. S. *Angew. Chem., Int. Ed.* **2013**, 9776−9780.
(89) Wagner, A.; Kaifer, E.; Himmel, H.-J. *Chem. Commun.* **2012**, *48*, 5277−5279.
(90) Carr, N.; Dunne, B. J.; Orpen, A. G.; Spencer, J. L. *J. Chem. Soc., Chem. Commun.* **1988**, 926−928.

DOI: 10.1021/ja510437p
J. Am. Chem. Soc. 2015, 137, 820−833

(91) Hasegawa, M.; Segawa, Y.; Yamashita, M.; Nozaki, K. *Angew. Chem., Int. Ed.* **2012**, *51*, 6956−6960.
(92) The synthesis, characterization, and reactivity of [**2-NBE**][$\mathbf{BAr^F_4}$] alongside detailed D-labeling experiments to deduce the mechansim of H_2 addition will be reported in a follow-up paper.
(93) Steed, J. W.; Atwood, J. L. *Supramolecular Chemistry*, 2nd ed.; John Wiley & Sons: Chichester, 2009.
(94) Siegel, J. S.; Anet, F. A. *J. Org. Chem.* **1988**, *53*, 2629−2630.
(95) Chierotti, M. R.; Gobetto, R. In *Supramolecular Chemistry: From Molecules to Nanomaterials*; Gale, P. A., Steed, J. W., Eds.; John Wiley & Sons: Hoboken, NJ, 2012.
(96) Wehrmann, F.; Albrecht, J.; Gedat, E.; Kubas, G. J.; Eckert, J.; Limbach, H. H.; Buntkowsky, G. *J. Phys. Chem. A* **2002**, *106*, 2855−2861.
(97) Gutmann, T.; del Rosal, I.; Chaudret, B.; Poteau, R.; Limbach, H.-H.; Buntkowsky, G. *ChemPhysChem* **2013**, *14*, 3026−3033.
(98) Smart, K. A.; Grellier, M.; Coppel, Y.; Vendier, L.; Mason, S. A.; Capelli, S. C.; Albinati, A.; Montiel-Palma, V.; Munoz-Hernandez, M. A.; Sabo-Etienne, S. *Inorg. Chem.* **2014**, *53*, 1156−1165.
(99) Le Roux, E.; Chabanas, M.; Baudouin, A.; de Mallmann, A.; Copéret, C.; Quadrelli, E. A.; Thivolle-Cazat, J.; Basset, J.-M.; Lukens, W.; Lesage, A.; Emsley, L.; Sunley, G. J. *J. Am. Chem. Soc.* **2004**, *126*, 13391−13399.
(100) Fulmer, G. R.; Miller, A. J. M.; Sherden, N. H.; Gottlieb, H. E.; Nudelman, A.; Stoltz, B. M.; Bercaw, J. E.; Goldberg, K. I. *Organometallics* **2010**, *29*, 2176−2179.
(101) Testing our NMR chemical shift calculations at the M06/SDD level shows a good agreement between experiment and computation for the previously reported (ref 49) [Rh(PONOP)(CH_4)]$^+$ system: δ −42 (exp), δ −40 (calcd).
(102) Brown, S. P.; Schaller, T.; Seelbach, U. P.; Koziol, F.; Ochsenfeld, C.; Klärner, F.-G.; Spiess, H. W. *Angew. Chem., Int. Ed.* **2001**, *40*, 717−720.
(103) Ochsenfeld, C.; Brown, S. P.; Schnell, I.; Gauss, J.; Spiess, H. W. *J. Am. Chem. Soc.* **2001**, *123*, 2597−2606.
(104) Woolf, A.; Chaplin, A. B.; McGrady, J. E.; Alibadi, M. A. M.; Rees, N.; Draper, S.; Murphy, F.; Weller, A. S. *Eur. J. Inorg. Chem.* **2011**, *2011*, 1614−1625.
(105) Freixa, Z.; Van Leeuwen, P. W. N. M. *Dalton Trans.* **2003**, 1890−1901.
(106) The diffraction pattern for [**4-NBA**][$\mathbf{BAr^F_4}$] suggested an incommenurately modulated structure: Palatinus, L.; Dusek, M.; Glaum, R. B.; El Bali, B. *Acta Crystallogr.* **2006**, *B62*, 556−566.
(107) Huang, D.; Huffman, J. C.; Bollinger, J. C.; Eisenstein, O.; Caulton, K. G. *J. Am. Chem. Soc.* **1997**, *119*, 7398−7399.
(108) Taw, F. L.; Mellows, H.; White, P. S.; Hollander, F. J.; Bergman, R. G.; Brookhart, M.; Heinekey, D. M. *J. Am. Chem. Soc.* **2002**, *124*, 5100−5108.
(109) Brookhart, M.; Green, M. L. H.; Parkin, G. *Proc. Natl. Acad. Sci. U.S.A.* **2007**, *104*, 6908−6914.
(110) Moxham, G. L.; Brayshaw, S. K.; Weller, A. S. *Dalton Trans.* **2007**, 1759−1761.
(111) Douglas, T. M.; Chaplin, A. B.; Weller, A. S. *Organometallics* **2008**, *27*, 2918−2921.
(112) Fryzuk, M. D. *Can. J. Chem.* **1983**, *61*, 1347−1351.
(113) Pike, S. D.; Pernik, I.; Theron, R.; McIndoe, J. S.; Weller, A. S. *J. Organomet. Chem.* **2014**, DOI: 10.1016/j.jorganchem.2014.08.012.
(114) See Supporting Materials in ref 59 for full details.
(115) Batool, M.; Martin, T. A.; Algarra, A. G.; George, M. W.; Macgregor, S. A.; Mahon, M. F.; Whittlesey, M. K. *Organometallics* **2012**, *31*, 4971−4979.
(116) Lein, M. *Coord. Chem. Rev.* **2009**, *253*, 625−634.
(117) The {P_2Rh(NBA)} fragment in the [**2-NBA**]$^+$ cation shows close to mirror symmetry, and so where relevant we only report QTAIM and NBO data for one of the near-symmetry-equivalent bonds. Computed differences are in all cases very small; see the Supporting Information.
(118) Popelier, P. L. A.; Logothetis, G. *J. Organomet. Chem.* **1998**, *555*, 101−111.
(119) Cremer, D.; Kraka, E. *Croat Chem. Acta* **1984**, *57*, 1259−1281.
(120) Sparkes, H. A.; Kramer, T.; Brayshaw, S. K.; Green, J. C.; Weller, A. S.; Howard, J. A. K. *Dalton Trans.* **2011**, *40*, 10708−10718.

DOI: 10.1021/ja510437p
J. Am. Chem. Soc. 2015, 137, 820−833